JPEDAV (2005) 26:131-151
DOI: 10.1361/15477030523021
1547-7037/$19.00 ©ASM International

Assessment of the La-Mn-O System

A. Nicholas Grundy, Ming Chen, Bengt Hallstedt, and Ludwig J. Gauckler

(Submitted November 7, 2003; in revised form January 8, 2005)

The particular relevance of the La-Mn-O system is due to the perovskite phase $La_{1-x}Mn_{1-y}O_{3-z}$, which, especially when doped with alkaline earth metals, is of interest both as cathode material for solid oxide fuel cells and its unusual giant magnetoresistive properties. Here, a complete thermodynamic description of all phases in the oxide part of the La-Mn-O system is presented. Particular focus is placed on modeling the defect chemistry of the perovskite phase. We used the compound energy model with the sublattice occupation (La^{3+}, Mn^{3+}, Va)(Mn^{2+}, Mn^{3+}, Mn^{4+}, Va)(O^{2-}, Va)$_3$. On reducing Mn^{3+} to Mn^{2+}, O vacancies are formed. On oxidation of Mn^{3+} to Mn^{4+}, equal numbers of vacancies are formed on the two cation sublattices while the O sublattice remains fully occupied. La-deficient perovskites have some Mn^{3+} substituting for La^{3+} on the A-site under reducing conditions. Under oxidizing conditions, more A-site vacancies are formed than B-site vacancies. Mn deficiency in perovskites can only be achieved by the formation of more vacancies on the B-sites than on the A-sites as La^{3+} does not substitute for Mn on the B-site. The ionic liquid is modeled using the two-sublattice model for ionic liquids. The phase La_2MnO_4 that is only stable above 1650 K and at low O partial pressures is described as a stoichiometric phase. Model parameters for the Gibbs energy functions are optimized according to the CALPHAD approach. No interaction parameters are necessary to give a good reproduction of all experimental data of the system.

1. Introduction

Doped lanthanum (La)-manganese (Mn) perovskites have for a long time attracted a lot of attention, first due to their rich variety of electrical and magnetic properties at low temperatures,[1-3] then due to their potential uses as sensors and catalysts.[4] The increased interest in solid oxide fuel cells (SOFCs) in the 1980s led to a renewed interest in doped La-Mn perovskites for use as cathode materials, because they are able to withstand the severe conditions encountered in SOFCs, have adequate electrical conductivity, show low overpotentials for oxygen (O) reduction at high temperatures, and, most importantly, are thermally, mechanically, and chemically compatible with yttria-stabilized zirconia (YSZ) electrolytes.[5,6] Recently, there has been yet another explosion of interest in lanthanum manganite perovskites with various dopants, due to the discovery of giant magnetoresistivity[7-9] or colossal magnetoresistivity[10,11] in these compounds. Magnetoresistance has also been found in undoped $LaMnO_{3+\delta}$.[12] All of these unique and interesting properties are strongly influenced by the defect chemistry of the perovskite phase. When modeling the perovskite phase, it is therefore of particular importance to model the defect chemistry as stringently as possible.

The La-Mn perovskite phase shows a well-established O nonstoichiometry and also a certain degree of deviation from the cation ratio of 1 to 1. As will be further elaborated, an O-deficient perovskite has O vacancies on the O sublattice, while a perovskite with a nominal O excess has in fact equal amounts of cation vacancies on the two-cation sublattices. La deficiency in the perovskite is caused by two mechanisms that dominate at different O partial pressures. Under oxidizing conditions, La vacancies are formed, and the charge deficiency that occurs is compensated for by the oxidation of Mn^{3+} to Mn^{4+}; under reducing conditions, some Mn^{3+} substitutes for La^{3+} on A-sites and the mean Mn valency remains unchanged. Mn deficiency occurs solely by the formation of B-site vacancies, as La cannot occupy Mn sublattice sites. Mn deficiency is therefore always accompanied by a sharp increase in the mean Mn valency. In view of this defect chemistry, the most correct way to write the chemical formula for the perovskite is $(La_{1-d}, Mn_d)_{1-x}Mn_{1-y}O_{3-z}$. On reduction of a stoichiometric perovskite, x, y, and d are ~0 and z is >0; on oxidation, x and y are >0, and z and d are ~0. An La-rich perovskite has $y > x$ and $d \sim 0$, and an Mn-rich perovskite has $x > y$ and/or $d > 0$, depending on the O partial pressure and temperature.

The stoichiometric perovskite displays a magnetic transition at ~150 K[13] and two structural phase transformations. The transformations that take place are an O′-orthorhombic → O-orthorhombic (O′ → O) transformation at ~750 K in air, which is caused by the loss of cooperative Jahn-Teller distortion of Mn^{3+} on increasing temperature and an O-orthorhombic → rhombohedral (O → R) transformation at ~1000 K in air.[14] These transitions are not considered further in this article.

Apart from the perovskite phase, the phase $La_2MnO_{4\pm\delta}$, which is isostructural[15] to the phase K_2NiF_4, is found in the La-Mn-O system above 1690 K. This phase was first synthesized by Vogel and Johnson[16] by reducing alkali-substituted $LaMnO_3$. The phase is only stable in reducing atmospheres.

Besides these two phases some other phases were claimed to have been synthesized. Seiler and Kaiser[17] produced the phase $LaMn_2O_4$ in air at low temperatures, Ned-

A. Nicholas Grundy, Ming Chen, and **Ludwig J. Gauckler,** Nonmetallic Inorganic Materials, Department of Materials, Swiss Federal Institute of Technology, Federal Institute of Technology, Zürich, Switzerland; and **Bengt Hallstedt,** Materials Chemistry, RWTH Aachen University, D-52056 Aachen, Germany. Contact e-mail: Nicholas.Grundy@mat.ethz.ch.

Table 1 Crystal structures of the phases found in the La-Mn-O system

Name	Composition	Space group	Structure type	Reference
O′-perovskite	$LaMnO_{3\pm d}$	*Pnma*	$GdFeO_3$	Elemans et al.[20]
O-perovskite	$LaMnO_{3\pm d}$	*Pnma*	$GdFeO_3$	Norby et al.[21]
R-perovskite	$LaMnO_{3\pm d}$	*R*3*c*	$LaAlO_3$	Norby et al.[21]
La_2MnO_4	La_2MnO_{4+d}	*14/mmm*	K_2NiF_4	Vogel and Johnson[16]

liko et al.[18] failed to synthesize this compound in the temperature range of 1073 to 1373 K. Bochu et al.[19] produced a phase of composition $LaMn_7O_{12}$ at 40 kbar pressure and 1273 K. As the stability of these phases is questionable, they are not considered further.

The crystal structures of the phases[20,21] $LaMnO_3$ and the phase La_2MnO_4[16] in the La-Mn-O system are summarized in Table 1.

This article presents a CALPHAD assessment of the La-Mn-O system. The thermodynamic parameters of the phases in the two binary border systems La-O[22] and Mn-O[23] were taken from previous optimizations. We ignore the La-Mn metallic binary system, as we are only interested in the oxide portion of the La-Mn-O system. We used the compound energy model[24,25] to describe the Gibbs energy of the perovskite phase, using the following sublattice occupation:

$$(La^{3+}, Mn^{3+}, Va)(Mn^{2+}, Mn^{3+}, Mn^{4+}, Va)(O, Va)_3$$

The model is based on the structural information of the phases and on its defect chemistry. The model parameters were optimized, giving a consistent description of all the experimental data that is related to the thermodynamics of the system. The Gibbs energy of the ionic liquid was modeled using the two-sublattice model for ionic liquids.[26,27] The phase La_2MnO_4 is modeled as a stoichiometric compound.

2. Literature Survey

2.1 The Perovskite $La_{1-x}Mn_{1-y}O_{3-z}$

2.1.1 Oxygen Nonstoichiometry of the Perovskite $La_{1-x}Mn_{1-y}O_{3-z}$. The O content in $La_{1-x}Mn_{1-y}O_{3-z}$ varies from hyper- to hypostoichiometric as a function of temperature and O partial pressure. Many of the important properties of $La_{1-x}Mn_{1-y}O_{3-z}$, such as catalysis, sinter behavior, electrical conductivity, and magnetism are strongly influenced by the defect chemistry of the phase. The O content of $La_{1-x}Mn_{1-y}O_{3-z}$ as a function of temperature and O partial pressure has been measured by many authors.[28-42] A change in O stoichiometry leads to a change in Mn valency. The average Mn valency as a function of temperature and O partial pressure has been measured by a number of authors using iodometric titration and similar methods.[43-52] Tanasescu et al.[53] measured the electromotive force (emf) of the perovskite with the O content adjusted by coulometric titration. A detailed review of the literature data on O nonstoichiometry is given below.

2.2 Oxygen-Deficient Region

On reducing the O partial pressure and/or increasing temperature, the perovskite loses O according to the following defect reaction:

$$2Mn_{Mn}^{x} + O_O^x \rightarrow 2Mn'_{Mn} + Va_O^{\cdot\cdot} + \frac{1}{2}O_2(g)$$

Oxygen deficiency as a function of O partial pressure and temperature has been measured by various authors.[31,35,36,40,41,51,53] In equilibrium with MnO and La_2O_3, $La_{1-x}Mn_{1-y}O_{3-z}$ shows a temperature-dependent O deficiency that has been measured by Kamata et al.,[54] Borlera and Abbattista,[55] and Atsumi et al.[56]

2.3 Oxygen Excess Region

Many interesting properties of the $La_{1-x}Mn_{1-y}O_{3-z}$ perovskite are based on the unusual capability of these compounds to show nominal O excess. Four different mechanisms of defect formation in O excess perovskites with $x(Mn) = x(La)$ are conceivable:

(1) The O occupies interstitial sites:

$$La_{La}^{x} + Mn_{Mn}^{x} + 3O_O^x + \frac{1}{4}O_2(g) \rightarrow La_{La}^{x} + Mn_{Mn}^{\cdot} + 3O_O^x + \frac{1}{2}O_i''$$

(2) Equal amounts of metal vacancies are formed on A- and B-sites:

$$\frac{6}{7}La_{La}^{x} + \frac{6}{7}Mn_{Mn}^{x} + \frac{18}{7}O_O^x + \frac{3}{14}O_2(g) \rightarrow \frac{6}{7}La_{La}^{x} + \frac{1}{7}Va_{La}''' + \frac{6}{7}Mn_{Mn}^{\cdot} + \frac{1}{7}Va_{Mn}''' + 3O_O^x$$

(3) Vacancies are formed on A (B)-sites exclusively. In this case, the migration of A (B) cations to complete the B (A) sublattice is necessary, thus forming antisite defects:

$$\frac{6}{7}La_{La}^{x} + \frac{6}{7}Mn_{Mn}^{x} + \frac{18}{7}O_O^x + \frac{3}{14}O_2(g) \rightarrow \frac{5}{7}La_{La}^{x} + \frac{2}{7}Va_{La}''' + \frac{6}{7}Mn_{Mn}^{\cdot} + \frac{1}{7}La_{Mn}^{x} + 3O_O^x$$

(4) Vacancies are formed only on one site. An oxide of the other cation precipitates as a second phase:

$$La_{La}^{x} + Mn_{Mn}^{x} + 3O_O^x + \frac{1}{2}O_2(g) \rightarrow \frac{2}{3}La_{La}^{x} + \frac{1}{3}Va_{La}''' + Mn_{Mn}^{\cdot} + 3O_O^x + \frac{1}{6}La_2O_3$$

or

$$La_{La}^{x} + Mn_{Mn}^{x} + 3O_{O}^{x} + \frac{1}{2}O_2(g) \rightarrow La_{La}^{x} + \frac{3}{4}Mn_{Mn}^{\cdot} + \frac{1}{4}Va_{Mn}''' + 3O_{O}^{x} + \frac{1}{4}MnO$$

In the literature there is general agreement that mechanism (1) is out of the question, because in the close-packed perovskite structure there are no interstitial sites large enough to accommodate interstitial O. This has been verified by a number of experimental methods, such as density measurements,[32,49,57] neutron diffraction,[37,58-62] and atomistic computer modeling of defect energies.[63] Most data from the literature agree on model (2), with equal numbers of metal vacancies on A- and B-sites. However, some authors also have reported unequal amounts of vacancies forming; however, none of them have given any indication as to where the superfluous ions get to (model 3 or 4). Below, the results obtained from the literature on O excess in perovskites with $x(\mathrm{Mn}) = x(\mathrm{La})$ are summarized.

In the work of Jonker and van Santen,[43] it was shown that $La_{1-x}Mn_{1-y}O_{3-z}$ is ferromagnetic only when it contains some Mn^{4+}, a property that was shown by Zener[1] to arise from a double-exchange process. This process causes the spins of the unpaired electron in adjacent Mn^{4+}-ions to align in parallel, thus causing ferromagnetism and simultaneously mediating ferromagnetic conductivity. Jonker and van Santen[43] determined the Mn^{4+} content as a function of temperature in air, Wold and Arnott[44] in O and in air, and Rubinchik et al.[45] in air. In one of the first investigations of the defect structure of $La_{1-x}Mn_{1-y}O_{3-z}$, Tofield and Scott[58] applied neutron diffraction to investigate $LaMnO_{3.12}$. By refining the diffraction patterns, they reached the conclusion that vacancies are formed on both cation sublattices, with more vacancies forming on the La sublattice. For this to be possible, they assumed that a small amount of La_2O_3 is precipitated on oxidation. Voorhoeve et al.[46] measured the Mn^{4+} content in air at 1173 K of samples with a cation ratio of 1 to 1. They assumed that on oxidation only La-vacancies are formed while the Mn and O sublattices remained fully occupied, also requiring the precipitation of La_2O_3. None of these authors, however, found any trace of La_2O_3. Kuo et al.[64] measured the change in O content as a function of temperature and O partial pressure using thermogravimetry, and described the defect chemistry of $La_{1-x}Mn_{1-y}O_3$ using equal amounts of vacancies on A- and B-sites ($x = y$) based on the results of Tofield and Scott.[58]

Further detailed experimental investigations of the defect chemistry of $La_{1-x}Mn_{1-y}O_3$ by van Roosmalen et al. [59] using neutron diffraction, high-resolution transmission electron microscopy, and density measurements,[57] also showed equal amounts of vacancies on A- and B-sites, which is in accordance with model 2. These authors found no defect clustering or crystallographic shear, indicating that vacancies are randomly distributed. The defect model they proposed[30,65] for $La_{1-x}Mn_{1-y}O_3$ contains equal numbers of La and Mn vacancies. They suggested that the results of the study by Tofield and Scott,[58] who used neutron diffraction and found more La vacancies than Mn vacancies in their cation-deficient sample, might have been due to the fact that their sample was La-deficient to start with and did not lose La on oxidation. Additionally, they proposed the occurrence of charge disproportionation of Mn^{3+} to explain the lack of dependence of electrical conductivity on O excess that was described in another article.[66] They assumed that in stoichiometric $LaMnO_3$ Mn^{+3} is to a significant extent disproportionated into Mn^{4+} and Mn^{2+}. With increasing oxidation ($x, y > 0, z \sim 0$), the amount of Mn^{4+} remains constant and Mn^{2+} is oxidized to Mn^{3+}. The charge-carrier concentration thus remains constant. Apart from the conductivity measurements, they further justified the disproportionation by the relatively unstable $3d^4$ electron configuration of Mn^{3+}.

Based on their measurements of electrical conductivity, Stevenson et al.[67,68] also reached the conclusion that there must be charge disproportionation. Using x-ray and electron diffraction and high-resolution electron microscopy, Hervieu et al.[50] found O excess to be realized with equal amounts of cation vacancies on A- and B-sites. They found their density measurements to confirm these findings. Neutron diffraction and refinement of site occupancies by Mitchell et al.[60] on undoped and Sr-doped perovskites showed that A-site occupancy is consistently lower than B-site occupancy. Based on this finding, which is the same as that of Tofield and Scott,[58] Yasumoto et al.[41] proposed that vacancies are formed predominantly on A-sites and that La forms antisite defects on the B-sublattice. However, they offered no experimental evidence of their own for this model. Mizusaki et al.[69] also assumed this defect model based on the results of Mitchell et al.[60] and on the fact that there are more reports in the literature on La diffusion than on Mn diffusion in $La_{1-x}Mn_{1-y}O_{3-z}$ perovskites. From this, they concluded that La diffusion is faster and therefore that A-site vacancy concentration must be higher than B-site vacancy concentration. Using atomistic simulation techniques, De Souza et al.[63] came to the conclusion that formal O excess in $LaMnO_{3+\delta}$, with $d > 0.105$, is realized by the formation of cation vacancies on both cation sublattices, with tendencies toward more La vacancies than Mn vacancies. They discounted the possibility of La forming antisite defects on the Mn sublattice (La_{Mn}^{x}) due to the high energies involved in such a defect. Using neutron powder diffraction on highly oxygenated samples, annealing at 200 bar O, Alonso et al.[61] found cation vacancies on both the La and Mn sublattices. They found substantially higher proportions of Mn vacancies. They were, however, not quite sure what happens to the excess Mn, because they found no trace of it their diffraction pattern. In a later article,[37] they again came to the same conclusion and proposed cation vacancies to be a function of O excess, showing that under more oxidizing conditions the number of Mn vacancies increases more rapidly than the number of La vacancies. Using their results, however, it can be easily calculated that >3 wt.% Mn oxide must be precipitated in the process, but no trace of it can be found in any of the diffraction or difference patterns. Huang et al.[62] found very slightly fewer La vacancies than Mn vacancies by refinement of their neutron diffraction data on cation-deficient $La_{1-x}Mn_{1-y}O_3$. Cook et al.[70] showed that their creep results on Sr-doped

$(La,Sr)_{1-x}Mn_{1-y}O_3$ can only be explained when the assumption is made that unequal numbers of A- and B-site vacancies are formed.

The experimental data by Mizusaki and colleagues[31,40] and Tagawa et al.[35] further suggest that the O excess (or rather the cation deficiency) does not exceed a maximum saturation value of $LaMnO_{3.18}$ at 873 K. They explained this by introducing a space around each vacancy in which no additional vacancies can occur. This is equivalent to a strong vacancy-vacancy repulsion. Nakamura and Ogawa[42] have proposed a similar model. Maurin et al.[71] also found a maximum O uptake when 30% of the Mn has a valency of 4+, corresponding to the composition $LaMnO_{3.15}$. Alonso et al.,[33] on the other hand, reached significantly higher O excess by measuring in high O pressures. Also Töpfer and Goodenough[51] found that at 1073 K in O_2, the achievement of equilibrium values for O content probably requires 4 days or more. This means that at 873 K equilibrium is reached only after prohibitively long equilibration times.

To summarize, many authors agree on a defect model by which equal numbers of vacancies are formed on both sublattices on the oxidation of the perovskite. There also have been, however, numerous reports on unequal numbers of vacancies being formed on the two-cation sublattices. However, no author has given a clear indication as to what happens to the excess ions, and no one has found any secondary oxide phase precipitating on oxidation. Conductivity measurements and other experimental evidence have suggested that Mn^{3+} disproportionates to some extent into Mn^{2+} and Mn^{4+}.

2.4 Cation Nonstoichiometry

Single-phase $La_{1-x}Mn_{1-y}O_{3-z}$ can be prepared with a certain range of cation nonstoichiometry. This is important for SOFC applications, because La-deficient perovskite cathodes, $La_{1-x}Mn_{1-y}O_{3-z}$, with $x > y$ in comparison with the stoichiometric perovskite, have been shown to have a higher stability toward YSZ electrolyte material.[72-75] Additionally, the electrical conductivity is increased,[66] the sinter curve is shifted to lower temperatures,[30] and La deficiency also positively influences the electrocatalytic properties of the perovskite.

2.4.1 Cation Nonstoichiometry in Equilibrium with La_2O_3 and MnO_x. The limits of solid solubility in air of the perovskite that is in equilibrium with La_2O_3 and MnO_x have been determined by a number of authors. The composition of $La_{1-x}MnO_3$ in equilibrium with Mn_3O_4 has been determined to be $x = 0.12$ (0.532 cation % Mn) and $x = 0.1$ (0.526 cation % Mn) in air at 1073 and 1573 K, respectively by Takeda et al.[29]; $x = 0.06$ (0.515 cation % Mn) in air at 1373 K by Habekost et al.[76]; and $x = 0.09$ (0.524 cation % Mn) at $p_{O2} = 10^{-7}$ bar and 1273 K, and in air at 1073 K by Sakai and Fjellvåg.[34] For $La_{1-x}La_{1-y}O_{3-z}$ in air at 1273 K, Töpfer and Goodenough[51] measured a maximum La deficiency of $x = 0.1$ (0.526 cation % Mn) and an Mn deficiency of at least $y = 0.1$ (0.474 cation % Mn). Hébert et al.[77] prepared Mn-deficient single-phase $LaMn_{1-y}O_3$, with $y = 0.1$ (0.474 cation % Mn), and Arulraj et al.[78] prepared single-phase samples of composition $La_{1-x}MnO_3$, with $x = 0.2$ (0.556 cation % Mn), and $LaMn_{1-y}O_3$, with $y = 0.2$ (0.444 cation % Mn), in air at 1223 K. This range of solid solubility is probably too high. In a more complete study, Van Roosmalen et al.[79] gave maximum solubility limits for both the La-rich and the Mn-rich phase boundaries of $La_{1-x}Mn_{1-y}O_{3\pm\delta}$. They found an average of $x = 0.09$ (0.524 cation % Mn), with no significant temperature dependence in equilibrium with MnO_x, and $y = 0.1$ (0.475 cation % Mn) in equilibrium with La_2O_3 at 1473 K, decreasing to 0.462 cation % Mn at 1273 K and 0.452 cation % Mn at 1123 K. In air, Zachau-Christiansen et al.[80] found an La deficiency in $La_{1-x}MnO_3$ in equilibrium with Mn_3O_4 of $x = 0.04$ (0.51 cation % Mn) up to 1273 K. On lowering the O pressure, they observed a reduction of the La deficiency. At an O pressure of $2.5\cdot10^{-9}$ bar, they found a composition of $La_{0.96}MnO_3$ (0.51 cation % Mn), at $2.7\cdot10^{-13}$ bar they found a composition of $La_{1.00}MnO_{2.99}$ (0.5 cation % Mn), and at $3\cdot10^{-17}$ bar they found a composition of $La_{1.02}MnO_{2.94}$ (0.495 cation % Mn). In other words, they found Mn deficiency to be in equilibrium with MnO. Bosak et al.[52] also stated that under oxidizing conditions the Mn solubility is increased, and under reducing conditions it is decreased. They gave solubility limits of $La_{0.7\text{-}0.8}MnO_3$ (0.556-0.588 cation % Mn) in air at 973 K, and $La_{0.8\text{-}0.9}MnO_3$ (0.526-0.556 cation % Mn) at $pO_2 = 5\cdot10^{-5}$ bar also at 973 K.

The following mechanisms can lead to cation nonstoichiometry:

- Unequal amounts of vacancies are formed on A and B sublattices.
- Antisite defects are formed.

According to Shannon,[81] the crystal radii of Mn^{3+} and La^{3+} in octahedral coordination are 0.785 Å (high spin) and 1.172 Å, respectively. The relatively large difference suggests that it is probably feasible only for Mn to sit on La sites, as La is too large to fit into the octahedral sites normally occupied by Mn. The crystal radius of Mn^{2+} in octahedral coordination is 0.97Å and is closer to the radius of La^{3+}. Therefore, it could also be possible that when Mn goes to an La site it has a tendency to be reduced to Mn^{2+}, thereby fitting better into the La site.

Using simultaneous Rietveld refinement of one x-ray and two neutron diffraction patterns, Habekost et al.[76] concluded that their sample of nominal composition $La_{0.85}MnO_3$ contained vacancies only on the La site. Sakai et al.[82] came to the same conclusion by applying the same experimental techniques to their sample of composition $La_{0.96}MnO_{3.05}$ and additionally ruled out the possibility of Mn entering La sites, because the opposite signs in neutron-scattering amplitudes for La and Mn would result in too low a refined La content. Cerva[83] used high-resolution transmission electron microscopy to study A-site-deficient $La_{0.8}Sr_{0.2}MnO_3$ and found vacancies on A-sites only. This all suggests that La deficiency leads to vacancies on the A-sublattice only. In contrast to this, Wolcyrz et al.[84] and Horyn et al.[85] came to the conclusion, using average Mn valency determination, density measurements,[85] and refinement of neutron powder diffraction,[84] that their La-

deficient sample with an La-to-Mn ratio of 0.91 to 1 equilibrated in air at 1270 K has in fact got the sublattice occupation $(La_{0.922}Mn_{0.013}Va_{0.065})MnO_3$. However, they also stated that the reliability factor of the refinement of their neutron powder diffraction pattern is equally good based on other assumed sublattice occupations that give the same average Mn valency. They concluded that neutron powder diffraction alone is not sufficient to determine the sublattice occupations, as the concentrations of ions on the respective sublattices are too small to significantly influence the diffraction pattern. Using x-ray diffraction and Rietveld refinement, Ferris et al.[32] found the anion sublattice to be fully occupied and found vacancies on both cation sublattices. In samples with small La-to-Mn ratios, they also mentioned the possibility of Mn sitting on La sites, albeit in small quantities. Further evidence of La vacancies forming in La-deficient $La_{1-x}MnO_{3\pm\delta}$ was provided by sinter rate measurements in air by von Roosmalen et al.[86] They found the highest sinter rates in La-deficient $La_{1-x}MnO_{3+\delta}$, intermediate sinter rates in stoichiometric $LaMnO_{3+\delta}$, and the lowest sinter rates in Mn-deficient $LaMn_{1-y}O_{3+\delta}$. Similar results were obtained by Stevenson et al.[87] and Berenov et al.[88] These findings correlate with the formation of La vacancies on the A-sublattice (model 1), leading to a higher La diffusion rate, and additionally suggest that La mobility is the rate-determining step in the overall ion diffusion. However, this does not rule out the formation of both antisite defects and vacancies on the A-site, as has been suggested by Wolcyrz et al.[84] and Ferris et al.[32]

2.4.2 Oxygen Nonstoichiometry in Perovskites with x(Mn) ≠ x(La). From the discussion above, it follows that it does not seem to be possible to determine the sublattice occupation based on the refinement of diffraction data alone, and one must resort to less direct methods. One such method is the measurement of the average Mn valency in combination with gravimetrically determined O nonstoichiometry data. If one assumes that antisite defects are formed, then a cation nonstoichiometric perovskite can have the identical average Mn valency as the stoichiometric one. If one assumes that the nonstoichiometry is due to the formation of additional cation vacancies on one of the two-cation sublattices and no antisite defects are allowed, then this forcibly leads to a charge deficiency when going from a stoichiometric to a La- or Mn-deficient perovskite. This charge deficiency is either compensated by the oxidation of Mn, thus increasing the average Mn valency that can be experimentally measured, or by the formation of O vacancies, which would change other physical properties of the perovskite, like the O diffusivity, that can also be experimentally measured. Thus, the oxidation behavior of cation nonstoichiometric perovskites delivers additional important information on the defect chemistry of these compounds. If one assumes that only Mn^{2+} fits into the La sites, then again charge compensation, albeit in a smaller magnitude than if vacancies with a nominal charge of zero are formed, is necessary.

Oxygen tracer diffusion measurements by Berenov et al.[88] indicated that La site deficiency has little effect on the O diffusion rate. This seems to speak against the formation of charge-compensating O defects and suggests either the formation of antisite defects with Mn^{3+} on La^{3+} sites or the oxidation of Mn^{3+} to Mn^{4+}. They added, however, their result could also have been caused by interactions between O and La vacancies, thus reducing the O mobility. Van Roosmalen et al.[79] have shown that the volume of the unit cell of $LaMnO_3$ decreases with increasing Mn^{4+} content and found a reduction of the unit cell volume of La-deficient samples. They stated that this supports the defect model in which vacancies are formed on the La sublattice and the charge deficit is compensated by the oxidation of Mn^{3+} to Mn^{4+}, thus reducing the lattice parameter. However, the unit cell volume would also be reduced if the smaller Mn^{3+} would substitute for La^{3+} on some A-sites. Ferris et al.[32] measured the O excess at 1123 and 1623 K in air for the La-deficient samples $La_{1-x}MnO_{3+\delta}$, with x = 0.05, 0.08, 0.1, 0.12, 0.15, and 0.2. They found that the Mn valency was increased for La-deficient samples, while the O sublattice remained fully occupied. However, the O excess they measured was much higher than that found in all other data from the literature, casting some doubt on the soundness of their data.

In contrast to these results, the extensive investigations of the compounds $LaMnO_{3\pm\delta}$, $La_{0.95}MnO_{3\pm\delta}$, and $La_{0.9}MnO_{3\pm\delta}$ by Mizusaki et al.,[31] using coulometric titration and iodometry combined with gravimetrically determined O nonstoichiometry, showed that the mean Mn valency as a function of temperature and O partial pressure is independent of La deficiency. This indicates that La deficiency is either accompanied by the formation of O vacancies or is caused by Mn forming antisite defects on the La sublattice. To model their experimental results, Mizusaki et al.[31] adopted the latter defect model. Zachau-Christiansen et al.[80] measured the O content of samples with the compositions $La_{0.96}MnO_{3\pm\delta}$, $La_{0.99}MnO_{3\pm\delta}$, and $La_{1.02}MnO_{3\pm\delta}$, and also found that the O content as a function of O partial pressure at 1273 K was similar for the three samples. They gave no indication as to the defect model that was at play. Sakai and Fjellvåg[34] assumed that the Mn valency remained constant and that vacancies were introduced into the O sublattice for their La-deficient samples. Using coulometric titration, Jena et al.[89] and Takeda et al.[29] found that the Mn valence was not influenced by La deficiency. Alonso[37] investigated $La_{1-x}MnO_3$ using neutron powder diffraction under oxidizing conditions and stated that increasing the La deficiency leads to an increasingly defective O sublattice. Töpfer and Goodenough[90] also stated that La deficiency leads to O vacancies, as did Pashchenko,[91] using x-ray diffraction and density measurements. Arulraj et al.[78] found that the mean Mn valency even decreased with increasing La deficiency. They explained this with the formation of additional O vacancies. They also determined the average Mn valency on increasing Mn deficiency and found it to increase sharply. Ippommatsu et al.[47] investigated $La_{1-x}MnO_3$, with x = 0.09, 0.10, and 0.11, treated in air and $p_{O2} = 10^{-7}$ at 1073 K. They stated that the mean Mn valency decreased on increasing La deficiency. Using electron spin resonance, they also discovered that Mn^{2+} was also present in the samples when the mean valency of Mn was >3. This suggests a certain degree of disproportionation ($Mn^{3+} \rightarrow Mn^{2+} + Mn^{4+}$). It could also mean that La defi-

ciency is caused by Mn^{2+} entering the La sublattice. Arulraj et al.[78] and Sakai and Fjellvåg[34] observed a decrease of Mn^{4+} content on increasing La deficiency. They explained this as the formation of extra O vacancies, which seems rather unlikely.

In one of the few investigations on Mn-deficient perovskites, Arulraj et al.[78] found that the average Mn valency on increasing Mn deficiency increases sharply. This can only be rationalized by the formation of vacancies on the Mn sublattice and charge compensation by partial oxidation of the remaining Mn.

2.4.3 Melting Point of the Perovskite Phase. The only data that exist on the melting of the perovskite is an estimation performed at 2173 K, probably in air, by King et al.[92]

3. The Phases $La_2MnO_{4+\delta}$, $LaMn_2O_5$, and Some Others

Borlera and Abbattista[55] reported the La_2MnO_{4+z} phase to be stable above 1655 K at low O partial pressures, with $z = 0.15$. The phase is of the K_2NiF_4 type and crystallizes in the *I*4/*mmm* space group. Vogel and Johnson[16] also reported to have been able to synthesize the phase under reducing atmospheric pressure, with K-substituted $LaMnO_3$ as a precursor. By performing experiments in sealed glass tubes, Borlera and Abbattista[55] found a four-phase equilibrium with MnO, La_2O_3, $LaMnO_{3-z}$, and $La_2MnO_{4.15}$ at 1653 K. Above this temperature, $La_2MnO_{4.15}$ is stable.

The phase $LaMn_2O_5$ that crystallizes in the space group *Pbam* has been synthesized under 200 bar O pressure by Alonso and colleagues.[93,94] Sieler and Kaiser[17] reported the synthesis of the more reduced form of this phase, $LaMn_2O_4$, at 1073 K under argon. Borlera and Abbattista,[55] on the other hand, were not able to confirm this finding. Nedilko et al.[18] did not manage to synthesize the phase in air between 1073 and 1373 K either.

Some additional phases also have been reported. Bochu et al.[19] reported the phase $LaMn_7O_{12}$, which they were able to synthesize at 1273 K under a pressure of 40 kbar. Abbattista and Borlera[95] found an ordering of vacancies in highly O-deficient phases, leading to the phases $La_8Mn_8O_{23}$ and $La_4Mn_4O_{11}$. The defect model proposed by Van Roosmalen and Cordfunke[96] considered the formation of O vacancy clusters. They believed that the interactions of these vacancy clusters led to the formation of the phases proposed by Abbattista and Borlera.[95]

4. Thermodynamic Data

The Gibbs energy of the reaction $La_2O_3 + MnO + O_2 \rightarrow LaMnO_{3-\delta}$ as a function of temperature has been determined either by emf measurements[53,97-100] or by direct determination of the dissociation pressure, either by determining the pressure at which there was a sudden weight loss[31,39,54,55,101-103] or there was a sudden change in conductivity.[103] Mizusaki et al.[31] found the dissociation pressure to be independent of La deficiency, a result that is perfectly logical because the equilibrium is still $La_{1-x}Mn_{1-y}O_{3-z}$ + MnO + La_2O_3, with just a little less La_2O_3 forming.

The enthalpy of formation of stoichiometric $LaMnO_3$ has been measured by Laberty et al.[104] by solution calorimetry yielding −1451.1 kJ mol^{-1} at 298 K. Rørmark et al.[105] also measured the heat of formation using the same method on samples of composition $LaMnO_{3.148}$ and $LaMnO_{3.045}$ and obtained values of −1435.4 and −1425.9 kJ mol^{-1}, respectively. Apart from these measurements, there have also been some estimations of the thermodynamic properties of $LaMnO_3$. Yokokawa et al.[106] estimated the $\Delta_f H$ at ~1425.1 kJ/mol and S at ~130.5 J/mol·K for $LaMnO_3$ at 298.15 K by considering ionic radii and Goldschmidt tolerance factors. For La_2MnO_x, they estimated the $\Delta_f H$ at ~2189 kJ/mol and S at ~210 J/mol·K.

The heat capacity of $LaMnO_3$ was measured by Satoh et al.[107] up to 750 K. Their heat capacity curve shows two thermal anomalies: one magnetic transition at 140 K, and a peak at 735 K resulting from the second-order O′ → O Jahn-Teller transition. Recently, Jacob and Attaluri[100] measured the heat capacity of $LaMnO_3$ between 400 and 1050 K. These measurements also showed a peak between 565 and 750 K resulting from the O′ → O Jahn-Teller transition. These transitions are not considered in this work. Suryanarayanan et al.[9] measured the heat capacity up to 350 K of $La_{0.85}MnO_3$ annealed in O at 1123 K, and in air at 1573 K.

5. Thermodynamic Modeling

5.1 The Ionic Liquid

The two-sublattice model for ionic liquids[26,27] that was used to describe the liquid phase was developed for liquids that show the ionic behavior of the components. The model follows the work of Temkin,[108] and assumes that the anions and cations occupy separate sublattices and are allowed to mix freely on their respective sublattice. Hypothetical vacancies are introduced on the anion sublattice to maintain charge neutrality and to allow the description of a metallic liquid containing cations only.

In the La-Mn-O system the model is represented as:

$$(La^{3+}, Mn^{2+}, Mn^{3+})_p(O^{2-}, Va^{q-})_q$$

It should be noted that Mn^{4+} is not included in the description. This is due to the fact that Mn^{4+} is stabilized in the perovskite phase, but probably only becomes stable in the liquid phase at very high O partial pressures. The number of sites on the respective sublattices, p and q, must vary with composition to maintain charge neutrality. The values of p and q are calculated by:

$$p = 2y_{O^{2-}} + qy_{Va^{-q}}$$

and

$$q = 3y_{La^{3+}} + 3y_{Mn^{3+}} + 2y_{Mn^{2+}}$$

where y represents the site fraction of a particular species on

the respective sublattice. The hypothetical vacancies have an induced charge of $-q$.

The molar Gibbs energy of the liquid is given by:

$$G_m^{Liq} = \sum_{i=\text{cations}} y_i y_{O^{2-}} {}^oG^{Liq}_{i:O^{2-}} + q \sum_{i=\text{cations}} y_i y_{Va^{q-}} {}^oG^{Liq}_{i:Va^{-q}} + RT \cdot \left(p \sum_{i=\text{cations}} y_i \ln y_i + q \sum_{j=\text{anions}} y_j \ln y_j \right) + {}^EG_m^{Liq}$$

The Gibbs energies of liquid Mn and La, ${}^oG^{Liq}_{Mn^{2+}:Va^{q-}}$ and ${}^oG^{Liq}_{La^{3+}:Va^{q-}}$, respectively, are taken from Dinsdale,[109] and the Gibbs energies of the oxides, ${}^oG^{Liq}_{Mn^{2+}:O^{2-}}$, ${}^oG^{Liq}_{Mn^{3+}:O^{2-}}$ and ${}^oG^{Liq}_{La^{3+}:O^{2-}}$ from previous assessments of the Mn-O system[23] and the La-O systems[22]. The excess Gibbs energy ${}^EG_m^{Liq}$ is given by

$$\begin{aligned}
{}^EG_m^{Liq} = {} & y_{Mn^{2+}} y_{Mn^{3+}} y_{O^{2-}} L^{Liq}_{Mn^{2+},Mn^{3+}:O^{2-}} + y_{Mn^{2+}} y_{La^{3+}} y_{O^{2-}} L^{Liq}_{Mn^{2+},La^{3+}:O^{2-}} \\
& + y_{Mn^{3+}} y_{La^{3+}} y_{O^{2-}} L^{Liq}_{Mn^{3+},La^{3+}:O^{2-}} + y_{Mn^{3+}} y_{O^{2-}} y_{Va^{q-}} L^{Liq}_{Mn^{3+}:O^{2-},Va^{q-}} \\
& + y_{Mn^{2+}} y_{O^{2-}} y_{Va^{q-}} L^{Liq}_{Mn^{2+}:O^{2-},Va^{q-}} + y_{La^{3+}} y_{O^{2-}} y_{Va^{q-}} L^{Liq}_{La^{3+}:O^{2-},Va^{q-}} \\
& + q y_{Mn^{2+}} y_{La^{3+}} y^2_{Va^{q-}} L^{Liq}_{Mn^{2+},La^{3+}:Va^{q-}} \\
& + q y_{Mn^{3+}} y_{La^{3+}} y^2_{Va^{q-}} L^{Liq}_{Mn^{3+},La^{3+}:Va^{q-}} \\
& + q y_{Mn^{3+}} y_{Mn^{2+}} y^2_{Va^{q-}} L^{Liq}_{Mn^{3+},Mn^{2+}:Va^{q-}} + \Sigma^E G^{Liq}_{ternaries}
\end{aligned}$$

and $\Sigma^E G^{Liq}_{ternaries}$ is given by:

$$\begin{aligned}
\Sigma^E G^{Liq}_{ternaries} = {} & y_{La^{3+}} y_{Mn^{2+}} y_{Mn^{3+}} y_{O^{2-}} L^{Liq}_{La^{3+},Mn^{2+},Mn^{3+}:O^{2-}} \\
& + q y_{La^{3+}} y_{Mn^{2+}} y_{Mn^{3+}} y^3_{Va^{q-}} L^{Liq}_{La^{3+},Mn^{2+},Mn^{3+}:Va^{q-}} \\
& + y_{La^{3+}} y_{Mn^{2+}} y_{O^{2-}} y_{Va^{q-}} L^{Liq}_{La^{3+},Mn^{2+}:O^{2-},Va^{q-}} \\
& + y_{La^{3+}} y_{Mn^{3+}} y_{O^{2-}} y_{Va^{q-}} L^{Liq}_{La^{3+},Mn^{3+}:O^{2-},Va^{q-}} \\
& + y_{Mn^{3+}} y_{Mn^{2+}} y_{O^{2-}} y_{Va^{q-}} L^{Liq}_{Mn^{3+},Mn^{2+}:O^{2-},Va^{q-}}
\end{aligned}$$

where the interaction terms L can be further expanded using Redlich-Kister-type polynomials.[110,111]

6. The Perovskite $La_{1-x}Mn_{1-y}O_{3-z}$

As described above, the $La_{1-x}Mn_{1-y}O_{3-z}$ perovskite must be described considering the following sublattice occupations if all possible nonstoichiometries are to be taken into account.

$$(La^{3+}, Mn^{3+}, Va)_1(Mn^{2+}, Mn^{3+}, Mn^{4+}, Va)_1(O^{2-}, Va)_3$$

In the framework of the compound energy model,[24,25] the Gibbs energy of this phase is the weighed sum of the 24 (not necessarily neutral!) possible endmember perovskites, plus an entropy term for ideal mixing of the ions and vacancies on the respective sublattices. The rather cumbersome expression for the Gibbs energy is given by:

$$\begin{aligned}
{}^oG^{Perov}_m = {} & y_{La^{3+}} y_{Mn^{3+}} y_{O^{2-}} {}^oG^{Perov}_{La^{3+}:Mn^{3+}:O^{2-}} \\
& + y_{La^{3+}} y_{Mn^{2+}} y_{O^{2-}} {}^oG^{Perov}_{La^{3+}:Mn^{2+}:O^{2-}} \\
& + y_{La^{3+}} y_{Mn^{4+}} y_{O^{2-}} {}^oG^{Perov}_{La^{3+}:Mn^{4+}:O^{2-}} + y_{La^{3+}} y_{Va} y_{O^{2-}} {}^oG^{Perov}_{La^{3+}:Va:O^{2-}} \\
& + y_{La^{3+}} y_{Mn^{3+}} y_{Va} {}^oG^{Perov}_{La^{3+}:Mn^{3+}:Va} + y_{La^{3+}} y_{Mn^{2+}} y_{Va} {}^oG^{Perov}_{La^{3+}:Mn^{2+}:Va} \\
& + y_{La^{3+}} y_{Mn^{4+}} y_{Va} {}^oG^{Perov}_{La^{3+}:Mn^{4+}:Va} + y_{La^{3+}} y_{Va} y_{Va} {}^oG^{Perov}_{La^{3+}:Va:Va} \\
& + y_{Mn^{3+}} y_{Mn^{3+}} y_{O^{2-}} {}^oG^{Perov}_{Mn^{3+}:Mn^{3+}:O^{2-}} \\
& + y_{Mn^{3+}} y_{Mn^{2+}} y_{O^{2-}} {}^oG^{Perov}_{Mn^{3+}:Mn^{2+}:O^{2-}} \\
& + y_{Mn^{3+}} y_{Mn^{4+}} y_{O^{2-}} {}^oG^{Perov}_{Mn^{3+}:Mn^{4+}:O^{2-}} \\
& + y_{Mn^{3+}} y_{Va} y_{O^{2-}} {}^oG^{Perov}_{Mn^{3+}:Va:O^{2-}} + y_{Mn^{3+}} y_{Mn^{3+}} y_{Va} {}^oG^{Perov}_{Mn^{3+}:Mn^{3+}:Va} \\
& + y_{Mn^{3+}} y_{Mn^{2+}} y_{Va} {}^oG^{Perov}_{Mn^{3+}:Mn^{2+}:Va} + y_{Mn^{3+}} y_{Mn^{4+}} y_{Va} {}^oG^{Perov}_{Mn^{3+}:Mn^{4+}:Va} \\
& + y_{Mn^{3+}} y_{Va} y_{Va} {}^oG^{Perov}_{Mn^{3+}:Va:Va} + y_{Va} y_{Mn^{3+}} y_{O^{2-}} {}^oG^{Perov}_{Va:Mn^{3+}:O^{2-}} \\
& + y_{Va} y_{Mn^{2+}} y_{O^{2-}} {}^oG^{Perov}_{Va:Mn^{2+}:O^{2-}} + y_{Va} y_{Mn^{4+}} y_{O^{2-}} {}^oG^{Perov}_{Va:Mn^{4+}:O^{2-}} \\
& + y_{Va} y_{Va} y_{O^{2-}} {}^oG^{Perov}_{Va:Va:O^{2-}} + y_{Va} y_{Mn^{3+}} y_{Va} {}^oG^{Perov}_{Va:Mn^{3+}:Va} \\
& + y_{Va} y_{Mn^{2+}} y_{Va} {}^oG^{Perov}_{Va:Mn^{2+}:Va} + y_{Va} y_{Mn^{4+}} y_{Va} {}^oG^{Perov}_{Va:Mn^{4+}:Va} \\
& + y_{Va} y_{Va} y_{Va} {}^oG^{Perov}_{Va:Va:Va} \\
& + RT \left[\begin{array}{l} (y_{La^{3+}} \ln y_{La^{3+}} + y_{Mn^{3+}} \ln y_{Mn^{3+}} + y_{Va} \ln y_{Va}) \\ + (y_{Mn^{4+}} \ln y_{Mn^{4+}} + y_{Mn^{3+}} \ln y_{Mn^{3+}} + y_{Mn^{2+}} \ln y_{Mn^{2+}} \\ + y_{Va} \ln y_{Va}) + 3(y_{O^{2-}} \ln y_{O^{2+}} + y_{Va} \ln y_{Va}) \end{array} \right] \\
& + {}^EG^{Perov}_m
\end{aligned}$$

The term ${}^EG^{Perov}_m$ represents the excess Gibbs energy that can be expanded, giving expressions that are similar to the ones for the liquid phase.

The challenge now is to assign values to the 24 ${}^oG$s that define the perovskite phase. It is clear that an optimization of an $A + BT$ term for each of the 24 ${}^oG$s is not required, because, (a) this would result in too many independent parameters and, (b) no experimental data could be directly assigned to any of the ${}^oG$s, as most of the ${}^oG$s (except for ${}^oG^{Perov}_{La^{3+}:Mn^{3+}:O^{2-}}$, ${}^oG^{Perov}_{Mn^{3+}:Mn^{3+}:O^{2-}}$ and ${}^oG^{Perov}_{Va:Va:Va}$) correspond to charged compounds that cannot physically exist. Therefore, the strategy we used to model the system was to choose appropriate neutral endpoints of the model that can be assigned to sets of experimental data and to allow a complete description of the system. All of the 24 ${}^oG$s were then rewritten using these neutral endpoints plus a combination of reciprocal relations. This strategy will now be explained in more detail.

Figure 1 shows a graphic representation of the model for the perovskite phase with 16 of the 24 ${}^oG$s marked. The remaining eight ${}^oG$s have Mn^{3+} instead of La^{3+} on the A-sites. Perovskites that lie on the shaded area labeled "neutral plane" have a zero net charge. The points at which the neutral plane intersects the edges of the cube correspond to possible neutral perovskite endpoints that could be used in the model. The following neutral perovskite endpoints were chosen to describe the system:

- $(La^{3+})(Mn^{3+})(O^{2-})_3$: stoichiometric perovskite
- $(La^{3+})(Mn^{2+})(O^{2-}_{5/6}, Va_{1/6})_3$: reduced stoichiometric perovskite

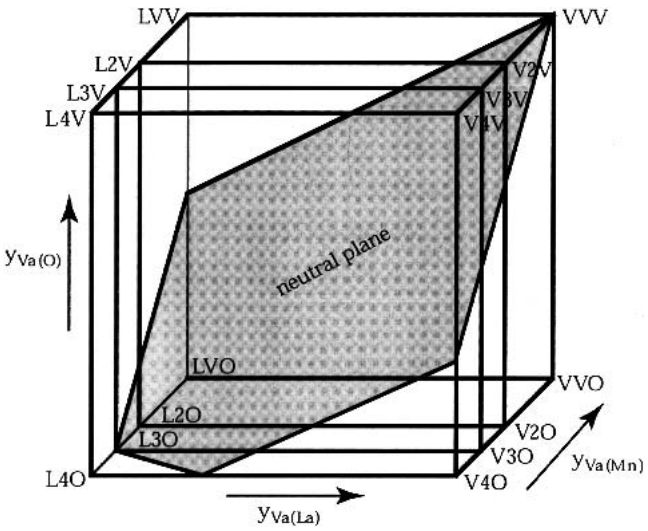

Fig. 1 Compositional space for the perovskite phase. Sixteen of the 24 ^{o}Gs are labeled in a shorthand fashion: L4O stands for $^{o}G^{Perov}_{La^{3+}:Mn^{4+}:O^{2-}}$ and so on. The remaining eight ^{o}Gs have Mn^{3+} instead of La^{3+} on the A-sites.

- $(La^{3+}_{2/3}, Va_{1/3})(Mn^{4+})(O^{2-})_3$: oxidized Mn rich perovskite
- $(La^{3+})(Mn^{4+}_{3/4}, Va_{1/4})(O^{2-})_3$: oxidized Mn deficient perovskite
- $(Va)(Va)(Va)_3$: perovskite consisting purely of vacancies.

The other neutral endpoints, which were not used are: $(La^{3+})(Va)(O^{2-}_{1/2}, Va_{1/2})_3$, La oxide in perovskite form, $(Va)(Mn^{2+})(O^{2-}_{1/3}, Va_{2/3})_3$, $(Va)(Mn^{3+})(O^{2-}_{1/2}, Va_{1/2})_3$, $(Va)(Mn^{4+})(O^{2-}_{2/3}, Va_{1/3})_3$; Mn oxides in perovskite form and $(La^{3+})(Mn^{2+}_{1/2}, Mn^{4+}_{1/2})(O^{2-})_3$, perovskite with Mn^{3+} completely dissociated into Mn^{2+} and Mn^{4+}; and corresponding endpoints with Mn^{3+} on the A-site. The composition range for which the perovskite phase is defined is shown as the shaded area in Fig. 2.

The five neutral endpoints used in the model description of the perovskite phase are marked in bold. The endmember $VaVaVa_3$ cannot be displayed in this representation.

First, we express the 16 ^{o}G parameters with no Mn^{3+} on the A-site using these 5 neutral endmembers, 10 reciprocal relations, and 1 arbitrary reference, giving a total of 16 equations. The first five equations can be given using the five chosen neutral endmembers:

$$^{o}G^{Perov}_{La^{3+}:Mn^{3+}:O^{2-}} = GL3O$$

$$\frac{5}{6}{}^{o}G^{Perov}_{La^{3+}:Mn^{2+}:O^{2-}} + \frac{1}{6}{}^{o}G^{Perov}_{La^{3+}:Mn^{2+}:Va} + 3RT\left[\frac{5}{6}\ln\left(\frac{5}{6}\right) + \frac{1}{6}\ln\left(\frac{1}{6}\right)\right] = GL2OV$$

$$\frac{2}{3}{}^{o}G^{Perov}_{La^{3+}:Mn^{4+}:O^{2-}} + \frac{1}{3}{}^{o}G^{Perov}_{Va:Mn^{4+}:O^{2-}} + 3RT\left[\frac{2}{3}\ln\left(\frac{2}{3}\right) + \frac{1}{3}\ln\left(\frac{1}{3}\right)\right] = GLV4O$$

$$\frac{3}{4}{}^{o}G^{Perov}_{La^{3+}:Mn^{4+}:O^{2-}} + \frac{1}{4}{}^{o}G^{Perov}_{La^{3+}:Va:O^{2-}} + 3RT\left[\frac{3}{4}\ln\left(\frac{3}{4}\right) + \frac{1}{4}\ln\left(\frac{1}{4}\right)\right] = GL4VO$$

$$^{o}G^{Perov}_{Va:Va:Va} = GVVV$$

The following reference was chosen:

$$^{o}G^{Perov}_{Va:Va:O^{2-}} = GVVV + \frac{3}{2}{}^{o}G^{Gas}_{O_2}$$

Finally, the following 10 reciprocal relations were used, giving the 16 equations required to calculate the 16 ^{o}G parameters:

$$\Delta G^{Perov}_{R1} = {}^{o}G^{Perov}_{La^{3+}:Mn^{3+}:O^{2-}} + {}^{o}G^{Perov}_{Va:Mn^{3+}:Va} - {}^{o}G^{Perov}_{La^{3+}:Mn^{3+}:Va} - {}^{o}G^{Perov}_{Va:Mn^{3+}:O^{2-}}$$

$$\Delta G^{Perov}_{R2} = {}^{o}G^{Perov}_{La^{3+}:Va:O^{2-}} + {}^{o}G^{Perov}_{Va:Va:Va} - {}^{o}G^{Perov}_{La^{3+}:Va:Va} - {}^{o}G^{Perov}_{Va:Va:O^{2-}}$$

$$\Delta G^{Perov}_{R3} = {}^{o}G^{Perov}_{La^{3+}:Mn^{2+}:O^{2-}} + {}^{o}G^{Perov}_{Va:Mn^{3+}:O^{2-}} - {}^{o}G^{Perov}_{La^{3+}:Mn^{3+}:O^{2-}} - {}^{o}G^{Perov}_{Va:Mn^{2+}:O^{2-}}$$

$$\Delta G^{Perov}_{R4} = {}^{o}G^{Perov}_{La^{3+}:Mn^{3+}:O^{2-}} + {}^{o}G^{Perov}_{Va:Mn^{4+}:O^{2-}} - {}^{o}G^{Perov}_{La^{3+}:Mn^{4+}:O^{2-}} - {}^{o}G^{Perov}_{Va:Mn^{3+}:O^{2-}}$$

$$\Delta G^{Perov}_{R5} = {}^{o}G^{Perov}_{La^{3+}:Mn^{4+}:O^{2-}} + {}^{o}G^{Perov}_{Va:Va:O^{2-}} - {}^{o}G^{Perov}_{La^{3+}:Va:O^{2-}} - {}^{o}G^{Perov}_{Va:Mn^{4+}:O^{2-}}$$

$$\Delta G^{Perov}_{R6} = {}^{o}G^{Perov}_{La^{3+}:Mn^{2+}:Va} + {}^{o}G^{Perov}_{Va:Mn^{3+}:Va} - {}^{o}G^{Perov}_{La^{3+}:Mn^{3+}:Va} - {}^{o}G^{Perov}_{Va:Mn^{2+}:Va}$$

$$\Delta G^{Perov}_{R7} = {}^{o}G^{Perov}_{La^{3+}:Mn^{3+}:Va} + {}^{o}G^{Perov}_{Va:Mn^{4+}:Va} - {}^{o}G^{Perov}_{La^{3+}:Mn^{4+}:Va} - {}^{o}G^{Perov}_{Va:Mn^{3+}:Va}$$

$$\Delta G^{Perov}_{R8} = {}^{o}G^{Perov}_{La^{3+}:Mn^{2+}:O^{2-}} + {}^{o}G^{Perov}_{La^{3+}:Mn^{3+}:Va} - {}^{o}G^{Perov}_{La^{3+}:Mn^{3+}:O^{2-}} - {}^{o}G^{Perov}_{La^{3+}:Mn^{2+}:Va}$$

$$\Delta G^{Perov}_{R9} = {}^{o}G^{Perov}_{La^{3+}:Mn^{3+}:O^{2-}} + {}^{o}G^{Perov}_{La^{3+}:Mn^{4+}:Va} - {}^{o}G^{Perov}_{La^{3+}:Mn^{4+}:O^{2-}} - {}^{o}G^{Perov}_{La^{3+}:Mn^{3+}:Va}$$

$$\Delta G^{Perov}_{R10} = {}^{o}G^{Perov}_{Va:Mn^{3+}:O^{2-}} + {}^{o}G^{Perov}_{Va:Va:Va} - {}^{o}G^{Perov}_{Va:Va:O^{2-}} - {}^{o}G^{Perov}_{Va:Mn^{3+}:Va}$$

Solving this system of equations for the 16 unknown ^{o}Gs gives the following result:

$$^{o}G^{Perov}_{La^{3+}:Mn^{3+}:O^{2-}} = GL3O$$

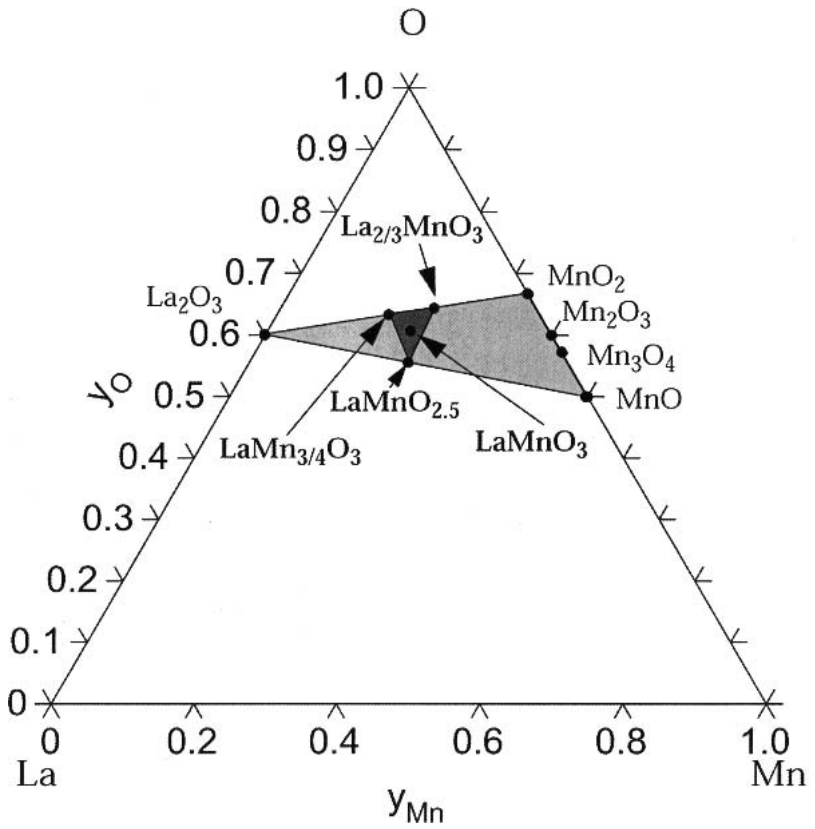

Fig. 2 Gibbs composition triangle of the La-Mn-O system showing the composition range (shaded) for which the perovskite phase is defined. The compositions marked in bold typeface are the perovskite endmembers that are used in the model description for the perovskite phase.

$$
{}^{o}G^{\text{Perov}}_{\text{La}^{3+}:\text{Mn}^{2+}:\text{O}^{2-}} = GL2OV + \frac{1}{4}G^{\text{Gas}}_{\text{O}_2} - 3RT\left[\frac{5}{6}\ln\left(\frac{5}{6}\right) + \frac{1}{6}\ln\left(\frac{1}{6}\right)\right] + \frac{1}{6}\Delta G^{\text{P}}_{\text{R1}} + \frac{1}{6}\Delta G^{\text{P}}_{\text{R8}} + \frac{1}{6}\Delta G^{\text{P}}_{\text{R10}}
$$

$$
{}^{o}G^{\text{Perov}}_{\text{La}^{3+}:\text{Mn}^{4+}:\text{O}^{2-}} = \frac{2}{3}GL4VO + \frac{1}{2}GLV4O - \frac{1}{6}GVVV - \frac{1}{4}G^{\text{Gas}}_{\text{O}_2} - \frac{2}{3}RT\left[\frac{3}{4}\ln\left(\frac{3}{4}\right) + \frac{1}{4}\ln\left(\frac{1}{4}\right)\right] - \frac{1}{2}RT\left[\frac{2}{3}\ln\left(\frac{2}{3}\right) + \frac{1}{3}\ln\left(\frac{1}{3}\right)\right] + \frac{1}{6}\Delta G^{\text{P}}_{\text{R5}}
$$

$$
{}^{o}G^{\text{Perov}}_{\text{La}^{3+}:\text{Va}:\text{O}^{2-}} = 2GL4VO - \frac{2}{3}GLV4O - \frac{1}{2}GVVV + \frac{3}{4}G^{\text{Gas}}_{\text{O}_2} - 2RT\left[\frac{3}{4}\ln\left(\frac{3}{4}\right) + \frac{1}{4}\ln\left(\frac{1}{4}\right)\right] + \frac{3}{2}RT\left[\frac{2}{3}\ln\left(\frac{2}{3}\right) + \frac{1}{3}\ln\left(\frac{1}{3}\right)\right] - \frac{1}{2}\Delta G^{\text{P}}_{\text{R5}}
$$

$$
{}^{o}G^{\text{Perov}}_{\text{La}^{3+}:\text{Mn}^{3+}:\text{Va}} = GL3O - \frac{3}{2}G^{\text{Gas}}_{\text{O}_2} - \Delta G^{\text{P}}_{\text{R1}} - \Delta G^{\text{P}}_{\text{R10}}
$$

$$
{}^{o}G^{\text{Perov}}_{\text{La}^{3+}:\text{Mn}^{2+}:\text{Va}} = GL2O - \frac{5}{4}G^{\text{Gas}}_{\text{O}_2} - 3RT\left[\frac{5}{6}\ln\left(\frac{5}{6}\right) + \frac{1}{6}\ln\left(\frac{1}{6}\right)\right] - \frac{5}{6}\Delta G^{\text{P}}_{\text{R1}} - \frac{5}{6}\Delta G^{\text{P}}_{\text{R8}} - \frac{5}{6}\Delta G^{\text{P}}_{\text{R10}}
$$

$$
{}^{o}G^{\text{Perov}}_{\text{La}^{3+}:\text{Mn}^{4+}:\text{Va}} = \frac{2}{3}GL4VO + \frac{1}{2}GLV4O - \frac{1}{6}GVVV - \frac{7}{4}G^{\text{Gas}}_{\text{O}_2} - \frac{2}{3}RT\left[\frac{3}{4}\ln\left(\frac{3}{4}\right) + \frac{1}{4}\ln\left(\frac{1}{4}\right)\right] - \frac{1}{2}RT\left[\frac{2}{3}\ln\left(\frac{2}{3}\right) + \frac{1}{3}\ln\left(\frac{1}{3}\right)\right] - \Delta G^{\text{P}}_{\text{R1}} + \frac{1}{6}\Delta G^{\text{P}}_{\text{R5}} + \Delta G^{\text{P}}_{\text{R9}} - \Delta G^{\text{P}}_{\text{R10}}
$$

$$
{}^{o}G^{\text{Perov}}_{\text{La}^{3+}:\text{Va}:\text{Va}} = 2GL4VO - \frac{2}{3}GLV4O + \frac{1}{2}GVVV - \frac{3}{4}G^{\text{Gas}}_{\text{O}_2} - 2RT\left[\frac{3}{4}\ln\left(\frac{3}{4}\right) + \frac{1}{4}\ln\left(\frac{1}{4}\right)\right] + \frac{3}{2}RT\left[\frac{2}{3}\ln\left(\frac{2}{3}\right) + \frac{1}{3}\ln\left(\frac{1}{3}\right)\right] - \Delta G^{\text{P}}_{\text{R2}} - \frac{1}{2}\Delta G^{\text{P}}_{\text{R5}}
$$

$$
{}^{o}G^{\text{Perov}}_{\text{Va}:\text{Mn}^{3+}:\text{O}^{2-}} = GL3O - 2GL4VO + \frac{2}{3}GLV4O + \frac{1}{2}GVVV + \frac{3}{4}G^{\text{Gas}}_{\text{O}_2} - 2RT\left[\frac{3}{4}\ln\left(\frac{3}{4}\right) + \frac{1}{4}\ln\left(\frac{1}{4}\right)\right] - \frac{3}{2}RT\left[\frac{2}{3}\ln\left(\frac{2}{3}\right) + \frac{1}{3}\ln\left(\frac{1}{3}\right)\right] - \Delta G^{\text{P}}_{\text{R4}} - \frac{1}{2}\Delta G^{\text{P}}_{\text{R5}}
$$

$$^{o}G^{Perov}_{Va:Mn^{2+}:O^{2-}} = GL2O - 2GL4VO + \frac{3}{2}GLV4O + \frac{1}{2}GVVV + G^{Gas}_{O_2} + 2RT\left[\frac{3}{4}\ln\left(\frac{3}{4}\right) + \frac{1}{4}\ln\left(\frac{1}{4}\right)\right] - \frac{3}{2}RT\left[\frac{2}{3}\ln\left(\frac{2}{3}\right) + \frac{1}{3}\ln\left(\frac{1}{3}\right)\right] - 3RT\left[\frac{5}{6}\ln\left(\frac{5}{6}\right) + \frac{1}{6}\ln\left(\frac{1}{6}\right)\right] + \frac{1}{6}\Delta G^{P}_{R1} - \Delta G^{P}_{R3} - \Delta G^{P}_{R4} - \frac{1}{2}\Delta G^{P}_{R5} + \frac{1}{6}\Delta G^{P}_{R8} + \frac{1}{6}\Delta G^{P}_{R10}$$

$$^{o}G^{Perov}_{Va:Mn^{4+}:O^{2-}} = 2GLV4O - \frac{4}{3}GL4VO + \frac{1}{3}GVVV + \frac{1}{2}G^{Gas}_{O_2} + \frac{4}{3}RT\left[\frac{3}{4}\ln\left(\frac{3}{4}\right) + \frac{1}{4}\ln\left(\frac{1}{4}\right)\right] - 2RT\left[\frac{2}{3}\ln\left(\frac{2}{3}\right) + \frac{1}{3}\ln\left(\frac{1}{3}\right)\right] - \frac{1}{3}\Delta G^{P}_{R5}$$

$$^{o}G^{Perov}_{Va:Va:O^{2-}} = GVVV + \frac{3}{2}G^{Gas}_{O_2}$$

$$^{o}G^{Perov}_{Va:Mn^{3+}:Va} = GL3O - 2GL4VO + \frac{3}{2}GLV4O + \frac{1}{2}GVVV - \frac{3}{4}G^{Gas}_{O_2} + 2RT\left[\frac{3}{4}\ln\left(\frac{3}{4}\right) + \frac{1}{4}\ln\left(\frac{1}{4}\right)\right] - \frac{3}{2}RT\left[\frac{2}{3}\ln\left(\frac{2}{3}\right) + \frac{1}{3}\ln\left(\frac{1}{3}\right)\right] - \Delta G^{P}_{R4} - \frac{1}{2}\Delta G^{P}_{R5} - \Delta G^{P}_{R10}$$

$$^{o}G^{Perov}_{Va:Mn^{2+}:Va} = GL2O - 2GL4VO + \frac{3}{2}GLV4O + \frac{1}{2}GVVV - \frac{1}{2}G^{Gas}_{O_2} + 2RT\left[\frac{3}{4}\ln\left(\frac{3}{4}\right) + \frac{1}{4}\ln\left(\frac{1}{4}\right)\right] - \frac{3}{2}RT\left[\frac{2}{3}\ln\left(\frac{2}{3}\right) + \frac{1}{3}\ln\left(\frac{1}{3}\right)\right] - 3RT\left[\frac{5}{6}\ln\left(\frac{5}{6}\right) + \frac{1}{6}\ln\left(\frac{1}{6}\right)\right] + \frac{1}{6}\Delta G^{P}_{R1} - \Delta G^{P}_{R4} - \frac{1}{6}\Delta G^{P}_{R5} - \Delta G^{P}_{R6} - \frac{5}{6}\Delta G^{P}_{R8} - \frac{5}{6}\Delta G^{P}_{R10}$$

$$^{o}G^{Perov}_{Va:Mn^{4+}:Va} = 2GLV4O - \frac{4}{3}GL4VO + \frac{1}{3}GVVV - G^{Gas}_{O_2} + \frac{4}{3}RT\left[\frac{3}{4}\ln\left(\frac{3}{4}\right) + \frac{1}{4}\ln\left(\frac{1}{4}\right)\right] - 2RT\left[\frac{2}{3}\ln\left(\frac{2}{3}\right) + \frac{1}{3}\ln\left(\frac{1}{3}\right)\right] - \Delta G^{P}_{R4} - \frac{1}{3}\Delta G^{P}_{R5} + \Delta G^{P}_{R7} + \Delta G^{P}_{R9} - \Delta G^{P}_{R10}$$

$$^{o}G^{Perov}_{Va:Va:Va} = GVVV$$

Table 2 Thermodynamic parameters for the La-Mn-O system

Perovskite phase $(La^{3+}, Va)(Mn^{2+}, Mn^{3+}, Mn^{4+}, Va)(O^{2-}, Va)_3$

$G_{LaMn^{3+}O_3} = GL3O = \frac{1}{2}{}^{o}G_{A\text{-}La_2O_3} + \frac{1}{2}{}^{o}G_{Mn_2O_3} - 63{,}367 + 51.77T - 7.19T\ln(T) + 232{,}934T^{-1}$

$G_{LaMn^{2+}(O_{5/6},Va_{1/6})_3} = GL2O = \frac{1}{2}{}^{o}G_{A\text{-}La_2O_3} + {}^{o}G_{MnO} + 27{,}672$

$G_{La(Mn^{4+}_{3/4}, Va_{1/4})O_3} = GL4VO = \frac{1}{2}{}^{o}G_{A\text{-}La_2O_3} + \frac{3}{4}{}^{o}G_{MnO_2} - 91{,}857 + 20.31T$

$G_{(La_{2/3},Va_{1/3})Mn^{4+}O_3} = GLV4O = \frac{1}{3}{}^{o}G_{A\text{-}La_2O_3} + {}^{o}G_{MnO_2} - 53{,}760$

$G_{VaVaVa_3} = GVVV = 6GL2O + 4GL4VO + 3GLV4O - 12GL3O - 254{,}212$

$ANTI = 547{,}422$

Ionic liquid $(La^{3+}, Mn^{2+}, Mn^{3+})_p(O^{2-}, Va^{-q})_q$

$^{o}L^{Liq}_{Mn^{3+},La^{3+}:O^{2-}} = {}^{o}L^{Liq}_{Mn^{2+},La^{3+}:O^{2-}} = -119{,}062$

La_2MnO_4

$G_{La_2MnO_4} = {}^{o}G_{A-La_2O_3} + {}^{o}G_{MnO} + 47{,}276 - 28.61T$

Note: All parameters are in SI units: J, mol, K; R = 8.31451 J/mol·K.

This manipulation leaves the following parameters to be optimized: *GL3O*, representing the stoichiometric perovskite $(La^{3+})(Mn^{3+})(O^{2-})_3$; *GL2O*, representing the reduced perovskite $(La^{3+})(Mn^{2+})(O^{2-}_{5/6}, Va_{1/6})_3$; *GLV4O*, representing the oxidized lanthanum deficient perovskite $(La^{3+}_{2/3}, Va_{1/3})(Mn^{4+})(O^{2-})_3$; *GL4VO*, representing the oxidized Mn deficient perovskite $(La^{3+})(Mn^{4+}_{3/4}\ Va_{1/4})(O^{2-})_3$; and *GVVV*, representing a perovskite that consists entirely of vacancies, $(Va)(Va)(Va)_3$. The values of these neutral endpoints are given relative to the sum of oxides corresponding to the composition of the neutral endpoint (Table 2). The neutral endpoint $VaVaVa_3$ (*GVVV*) is based on a Wagner-Shottky expression. The choice of this expression significantly facilitates the optimization and leads to a smaller sum of squared errors compared with other expressions for the vacancy energy, such as setting $GVVV = GL3O + A + BT$, or simply using the linear expression $GVVV = A + BT$. What then remains are the eight ^{o}Gs that have Mn^{3+} instead of La^{3+} on the A-site. These eight ^{o}Gs are given by an expression that is identical to those of the corresponding eight ^{o}Gs with La^{3+} on the A-site plus an antisite energy, termed *ANTI*. The parameter $^{\circ}G^{Perov}_{La^{3+}:Mn^{3+}:O^{3-}}$ for stoichiometric perovskite then becomes:

$$^{o}G^{Perov}_{Mn^{3+}:Mn^{3+}:O^{2-}} = GL3O + ANTI$$

and for corresponding equations for the other seven ^{o}Gs with La^{3+} on the A-site.

7. The Phase La_2MnO_4

Very little is known about this phase. The reason is that it is only stable at low O partial pressures and decomposes below 1653 K.[55] In air, it is not stable at all. Even though there have been reports of the phase having a certain O

excess,[55] not enough is known for it to make sense to model it. Yokokawa et al.[106] estimated the enthalpy of formation and the entropy of the phase, and Tanasescu[112] conducted some unpublished emf measurements that indicated the formation of the phase at high temperatures and low O partial pressure.

8. Optimization of Parameters

The thermodynamic parameters were optimized using the PARROT module of the Thermo-Calc[113] database system by minimizing the sum of squared errors between experimentally determined thermodynamic and phase diagram data taken from the literature and the corresponding calculated data.

8.1 The Ionic Liquid

The only datapoint concerning the liquid phase was the estimated melting point of the perovskite in air[92] at 2173 K. We optimized the same value for the interaction between La^{3+} and Mn^{3+}, which pertains to an oxidized oxidic melt, and between La^{+3} and Mn^{+2}, which becomes important for a reduced oxidic melt. The metallic melt (with Va on the second sublattice) is described as ideal due to the complete lack of experimental data.

8.2 The Perovskite $La_{1-x}Mn_{1-y}O_{3-z}$

8.2.1 Thermodynamic Data. The Gibbs energy of the reaction $\frac{1}{2}La_2O_3 + MnO + \frac{1}{4}O_2 = LaMnO_{3-z}$ measured by Jacob and Attaluri[100] was used for the optimization, because this data is very recent and covers a wide temperature range, and we have found that experiments from this group were carefully executed and reliable. Additionally, the heats of formation, measured by Laberty et al.[104] and Rørmark et al.[105] were used; however, these were given a smaller weight. These thermodynamic data mainly determined the parameter $A + BT$ of the function *GL3O* that describes the Gibbs energy of stoichiometric $LaMnO_3$ as a function of temperature. The heat capacity measured by Jacob and Attaluri[100] was found to deviate significantly from the Neumann-Kopp rule, and the two parameters $CT\ln(T) + D/T$ in *GL3O* were optimized to reproduce the measured data.

8.2.2 Phase Diagram Data. The La deficiency of $La_{1-x}Mn_{1-y}O_{3-z}$, in equilibrium with MnO_x, and the Mn deficiency, in equilibrium with La_2O_3, which were measured by van Roosmalen et al.[79] in air, by Zachau-Christiansen et al.[80] under low O partial pressure, and by Bosak et al.[52] in air and under low O partial pressure, were used for the optimization. The O deficiency in $LaMnO_{3-z}$ for the three-phase equilibrium $La_2O_3 + MnO + LaMnO_{3-z}$ measured by Borlera and Abbattista,[55] Kamata et al.,[54] and Atsumi et al.[56] was also used.

8.2.3 Oxygen Nonstoichiometry Data. Oxygen nonstoichiometry data constitute the main bulk of experimental data on the $La_{1-x}Mn_{1-y}O_{3-z}$ phase.

For this optimization, we chose to use the data from Mizusaki et al.[31] for stoichiometric and La-deficient perovskite, because these data seemed to agree quite well with most other data and a large number of data points are

Table 3 Measured thermodynamic properties of the phases in the La-Mn-O system compared to the calculated values

Phase	Composition	Quantity	Method	Value	Reference
Perovskite	$LaMnO_3$	$\Delta^\circ_f H298$	Solution calorimetry	−1451.1 kJ/mol (−72.1 kJ/mol)	Laberty et al.[104]
Perovskite	$LaMnO_{3.148}$	$\Delta^\circ_f H298$	Solution calorimetry	−1435.4 kJ/mol (−56.4 kJ/mol)	Rømark et al.[105]
Perovskite	$LaMnO_{3.045}$	$\Delta^\circ_f H298$	Solution calorimetry	−1425.9 kJ/mol (−46.9 kJ/mol)	Rømark et al.[105]
Perovskite	$LaMnO_3$	$\Delta^\circ_f H298$	Estimated	−1425.1 kJ/mol (−46.1 kJ/mol)	Yokoawa et al.[106]
Perovskite	$LaMnO_3$	$\Delta^\circ_f H298$	Assessed	−1438.7 kJ/mol (−59.7 kJ/mol)	This work
La_2MnO_4	La_2MnO_4	$\Delta^\circ_f H298$	Estimated	−2189 kJ/mol (+87.8 kJ/mol)	Yokokawa et al.[106]
La_2MnO_4	La_2MnO_4	$\Delta^\circ_f H298$	Assessed	−2135 kJ/mol (+141.8 kJ/mol)	This work
Perovskite	$LaMnO_3$	$^\circ S_{298}$	Estimated	130.5 J/mol·K (−73.4 J/mol·K)	Yokoawa et al.[106]
Perovskite	$LaMnO_3$	$^\circ S_{298}$	Assessed	118.7 J/mol·K (−73.4 J/mol·K)	This work
La_2MnO_4	La_2MnO_4	$^\circ S_{298}$	Estimated	210 J/mol·K (−140 J/mol·K)	Yokokawa et al.[106]
La_2MnO_4	La_2MnO_4	$^\circ S_{298}$	Assessed	215 J/mol·K (−135 J/mol·K)	This work

Notes: The values in parentheses are given relative to the oxides Mn_2O_3 and La_2O_3 using the heats and entropies of formation reported for the binary Mn-O[23] and La-O[22] systems

reported. The few data points from Mizusaki et al.[31] at 873 K and high O partial pressure, which indicated that the O excess in the perovskite does not go beyond a certain level, were, however, ignored because they contradict the data of Verelst et al.[48] and Alonso et al.[33] The O excess data of Alonso et al.[33] at high O partial pressures, and the O excess data of La-deficient and Mn-deficient perovskites measured by Zachau-Christiansen et al.[80] and Arulraj et al.[78] were also used for the optimization, because these data were the only data of this kind and were complementary to the data of Mizusaki et al.[31]

In view of their strong interdependence, all parameters for the perovskite phase need to be optimized simultaneously. Once good starting values have been ascertained, this can be done without difficulty. There are a large number of possible interaction parameters that could also be used to refine the optimization. However, this was not necessary, because all data on the system could be reproduced well within the uncertainties of the experimental data using only the parameters *GL3O*, *GL2O*, *GLV4O*, *GL4VO*, and *GVVV*, which were defined above and the values for which are given in Table 2.

8.3 The Phase La_2MnO_4

The parameters for the phase La_2MnO_4 (Table 2) were optimized using the decomposition temperature of 1653 K,[55] and the estimated enthalpy of formation and entropy of the phase of Yokokawa et al.[106] Also the unpublished emf data from the study by Tanasescu[112] were used, which were measured for the reaction:

$$\frac{1}{2}La_2O_3 + LaMnO_3 \rightarrow La_2MnO_4 + \frac{1}{4}O_2(g).$$

The heat capacity of the phase La_2MnO_4 was not optimized, and is given as a linear combination of the phases MnO and La_2O_3 according to the Neumann-Kopp rule.

9. Results and Discussion

The optimized thermodynamic parameters describing the La-Mn-O system are listed in Table 2.

9.1 Thermodynamic Data

The calculated heats of formation ΔH_f^o of the phases in the La-Mn-O system are compared with data from the literature in Table 3.

The calculated heat capacity of stoichiometric $LaMnO_3$ is compared with the measured values of Satoh et al.[107] and Jacob and Attaluri[100] in Fig. 3. The dashed line corresponds to the heat capacity calculated as $c_P(LaMnO_3) = \frac{1}{2}c_P(La_2O_3) + \frac{1}{2}c_P(Mn_2O_3)$ according to the Neumann-Kopp rule. The data from Jacob and Attaluri[100] were used for the optimization and were found to deviate significantly from the Neumann-Kopp rule. The calculated Gibbs energy, recalculated as $\log(P_{O2})$ of the reaction $\frac{1}{2}La_2O_3 + MnO + \frac{1}{4}O_2 = LaMnO_3$, is plotted as a function of the inverse temperature in Fig. 4 and is compared with the experimental data. The data from the study by Jacob and Attaluri[100] are reproduced very well by this optimization. The dissociation pressure measurements made by Mizusaki et al.,[31] which

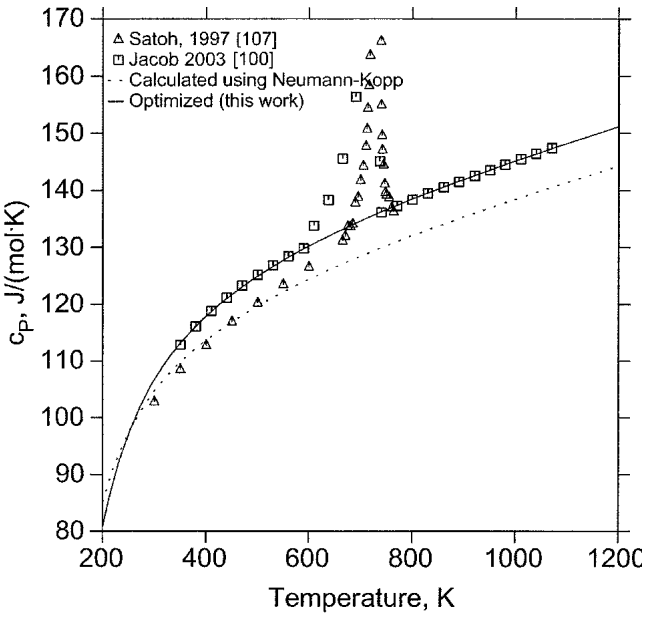

Fig. 3 The heat capacity, C_p, measured by Jacob and Attaluri,[100] was used in this optimization. The dashed line is the heat capacity calculated using the Neumann-Kopp rule. The anomaly in the experimental data was caused by the O′-R phase transition, which was not considered in this work.

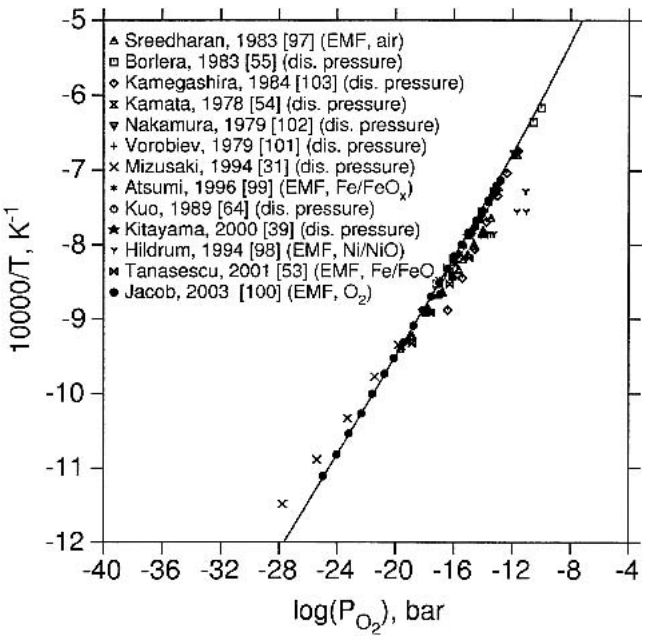

Fig. 4 Experimentally determined Gibbs energy for the reaction $\frac{1}{2}La_2O_3 + MnO + \frac{1}{4}O_2(g) = LaMnO_3$ displayed as dissociation pressure as a function of inverse temperature compared with the calculated curve

Table 4 Gibbs energy of the reaction $\frac{1}{2}$ La_2O_3 + MnO + $\frac{1}{4}$ O_2(g) = $LaMnO_3$

T range, K	$\Delta^oG(T)$, J/mol	Method	Reference
1050-1300	−16,167 + 65*T*	emf (gas mixture)	Sreedharan et al.[97]
1273	−91,700	Dissociation pressure	Nakamura et al.[102]
1223-1323	−90,026 + 21.07*T*	Dissociation pressure	Vorob'ev et al.[101]
1173-1523	−144,000 + 41*T*	Dissociation pressure	Borlera and Abbattista[55]
1173-1473	−130,900 + 32.9*T*	Conductivity measure	Kamegashira et al.[103]
1170-1400	−140,300 + 39.1*T*	emf (Fe/FeOx)	Atsumi et al.[99]
1073-1273	−167,740 + 65*T*	emf (Fe/FeOx)	Tanasescu et al.[53]
1473	−82,140	Dissociation pressure	Kamata et al.[54]
1473	−83,900	Dissociation pressure	Kuo et al.[64]
1373	−85,800	Dissociation pressure	Kitayama[39]
1273-1373	−197,800 + 91*T*	emf (Ni/NiO)	Hildrum et al.[98]
873-1273	−170,200 + 63.8*T*	Dissociation pressure	Mizusaki et al.[31]
900-1400	−144,290 + 42.68*T*	emf (oxygen)	Jacob and Attaluri[100]
900-1500	−141,905 + 39*T*	Assessed	This work

Table 5 Calculated temperatures of three-phase equilibria in air and at 1 bar O_2, and invariant four-phase equilibria

Equilibrium	Calculated temperature, K	Calculated O partial pressure, bar
A-La_2O_3 + liquid + perovskite in air	2096 (2130)	Air (1 bar O_2)
β-Mn_3O_4 + liquid + perovskite in air	1791 (1823)	Air (1 bar O_2)
Congruent melting point of perovskite in air	2173 (2228)	Air (1 bar O_2)
$Mn_{1-x}O$ + La_2MnO_4 + perovskite + liquid	1287	$10^{-15.85}$
β-Mn_3O_4 + $Mn_{1-x}O$ + perovskite + liquid	1740	$10^{-1.64}$
$Mn_{1-x}O$ + A-La_2O_3 + La_2MnO_4 + perovskite	1655	$10^{-9.96}$

Values in parentheses are temperature measured in O_2.

deviate considerably from the measurements of Jacob and Attaluri[100] at low temperatures, cannot be reproduced, because they would require an unreasonable curvature of the $\log(P_{O2})$ versus $1/T$ curve. Linear equations of the partial Gibbs energy as a function of temperature are compared with data from the literature in Table 4.

The calculated temperatures of three phase equilibria in air and 1 bar O_2 and invariant four-phase equilibria are listed in Table 5.

9.2 The Phase Diagram

Isothermal sections of the system of the systems $LaO_{1.5}$-MnO_2-MnO at 1973, 1473, and 1073 K are shown in Fig. 5 to 7.

We chose the oxides as corners of the ternary section because no information on the metallic binary La-Mn system is available, and we were only interested in the oxide portion of the system. The following equations can be used to calculate the mole fractions $x(\mathrm{MnO})$, $x(\mathrm{MnO_2})$, and $x(\mathrm{LaO_{1.5}})$ using $x(\mathrm{Mn})$ and $x(\mathrm{La})$:

$$x(\mathrm{MnO}) = \frac{3x(\mathrm{Mn}) + 2.5x(\mathrm{La}) - 1}{x(\mathrm{Mn}) + x(\mathrm{La})}$$

$$x(\mathrm{MnO_2}) = \frac{1 - 2x(\mathrm{Mn}) - 2.5x(\mathrm{La})}{x(\mathrm{Mn}) + x(\mathrm{La})}$$

$$x(\mathrm{LaO_{1.5}}) = \frac{x(\mathrm{La})}{x(\mathrm{Mn}) + x(\mathrm{La})}$$

The dashed lines through the ternary sections represent the composition path calculated at O partial pressures of 0.21 bar (air) and 1 Pa. It is evident that the range of cation nonstoichiometry decreases on the lowering of the O partial pressure. This is in qualitative agreement with the observations by Zachau-Christiansen et al.[80] and Bosak et al.[52]

Figure 8 shows the calculated $LaO_{1.5}$-MnO_x phase diagram in air, with some experimental data points included. The experiments suggest that the range of solid solubility decreases with increasing temperature. The Mn^{4+} content also decreases with increasing temperature, which is in agreement with the decreased range of solid solubility with decreasing the O partial pressure, and thus with the decreasing Mn^{4+} content that can be observed in the ternary sections (Fig. 5-7). Figure 9 shows the $LaO_{1.5}$-MnO_x phase diagram calculated at an O partial pressure of 1 Pa (10^{-5} bar). It can be seen that the range of solid solubility of $La_{1-x}Mn_{1-y}O_{3-z}$ is reduced, as is its melting point.

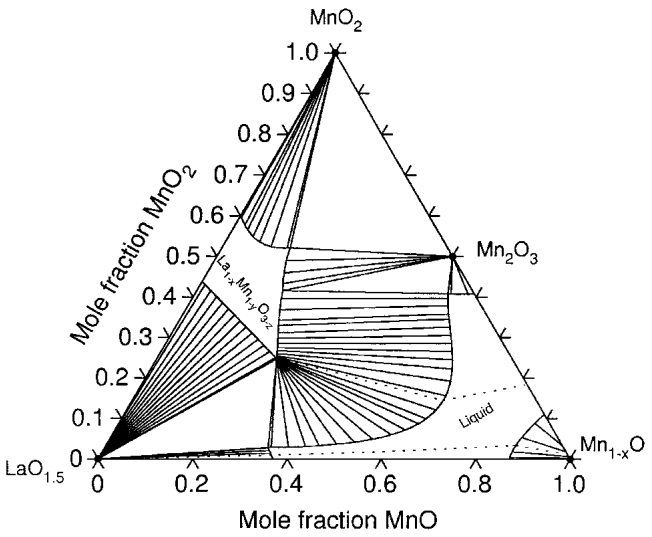

Fig. 5 Isothermal section of the La-Mn-O phase diagram at 1973 K. The dashed lines correspond to the O content in air and in 1 Pa O_2.

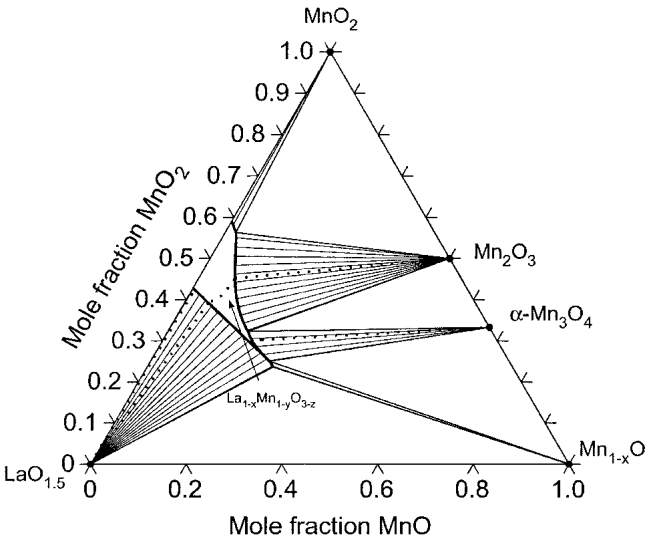

Fig. 7 Isothermal section of the La-Mn-O phase diagram at 1073 K. The dashed lines correspond to the O content in air and in 1 Pa O_2.

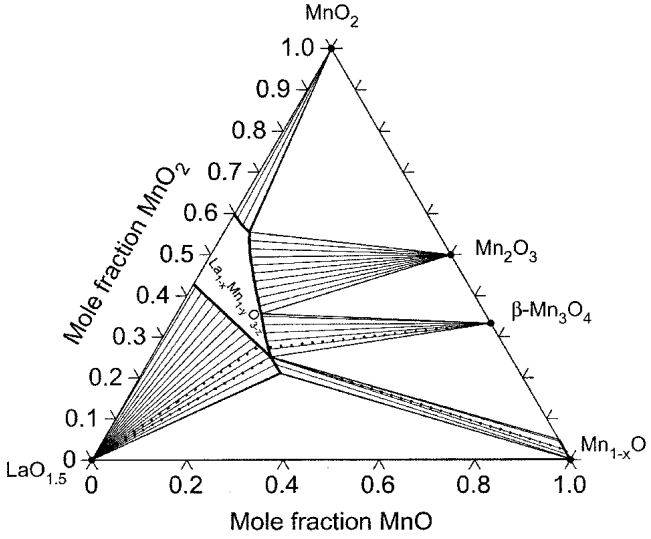

Fig. 6 Isothermal section of the La-Mn-O phase diagram at 1473 K. The dashed lines correspond to the O content in air and in 1 Pa O_2.

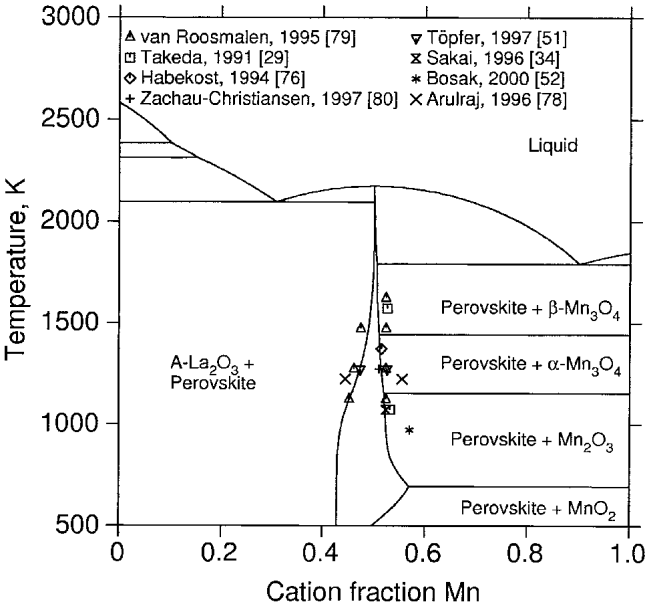

Fig. 8 The $LaO_{1.5}$-MnO_x phase diagram calculated in air with experimental data included

The calculated temperatures of the invariant three-phase equilibria in air and the invariant four phase equilibria in the La-Mn-O system are listed in Table 5.

The O content in $LaMnO_{3-z}$ in equilibrium with La_2O_3 and MnO as a function of temperature is compared with the calculated content in Fig. 10. This equilibrium corresponds to the one used in Fig. 4 showing the O potential as a function of temperature. The deviation between the calculated curve and the experimental data is due to the fact that there have been a large number of experiments (Fig. 11-17) that have clearly shown that considerable O deficiency also is observed before the perovskite decomposes at low temperatures.

The calculated O contents as a function of temperature and the O partial pressure for stoichiometric $LaMnO_{3\pm\delta}$, $La_{0.9}MnO_{3\pm\delta}$, and $LaMn_{0.9}O_{3\pm\delta}$ are compared with data from the literature in Fig. 11 to 17. It should be noted that $La_{0.9}MnO_{3\pm\delta}$ is beyond the cation solubility limits under reducing conditions. However, when Mizusaki et al.[31] reduced the O partial pressure, no MnO_x was precipitated, because this would have led to discontinuous jumps in the O content versus O partial pressure curves that they did not observe. This means that the phase was conserved in a metastable state for the duration of the experiments. Also

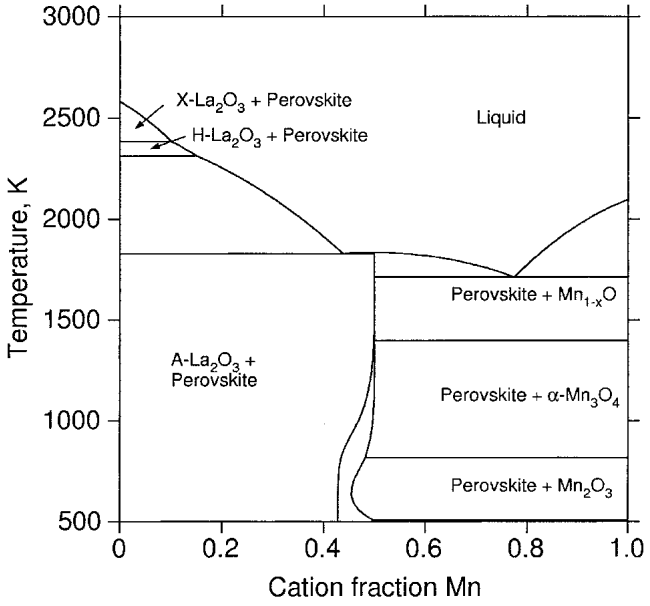

Fig. 9 Pseudobinary section calculated at an O partial pressure of 1 Pa through the La-Mn-O system. It can be seen that, in equilibrium with MnO_x, the perovskite shows an Mn deficiency, a result that has been experimentally verified.[80]

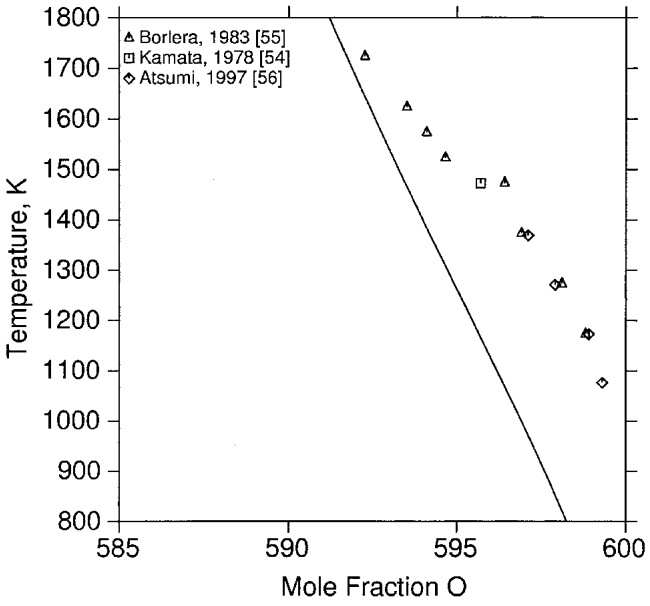

Fig. 10 The O content of $LaMnO_{3-\delta}$ in equilibrium with MnO and La_2O_3 as a function of temperature

$LaMn_{0.9}O_{3\pm\delta}$ is metastable under reducing conditions. For this Mn-deficient perovskite, only one experiment on O nonstoichiometry concerning the function of temperature and O partial pressure exists. In Fig. 14 it can be seen that this measurement of O content by Arulraj et al.[78] is higher than those for both a stoichiometric and an La-deficient perovskite (arrow). This is in qualitative agreement with the calculated curves. In Fig. 18, the O content as a function of temperature in air and in O_2 is shown. There are quite a

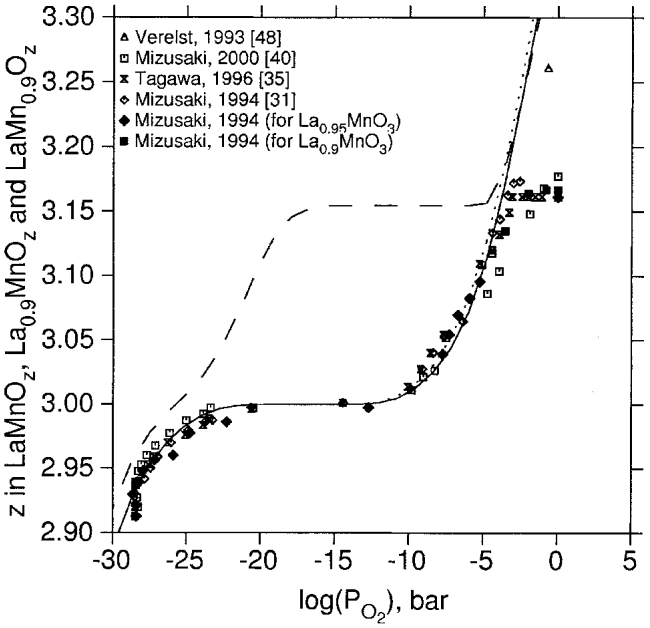

Fig. 11 The O content of $LaMnO_{3\pm\delta}$ (solid line), $LaMn_{0.9}O_{3\pm\delta}$ (dashed line), and $La_{0.9}MnO_{3\pm\delta}$ (dotted line) calculated as a function of $\log(P_{O2})$ at 873 K compared with data from the literature

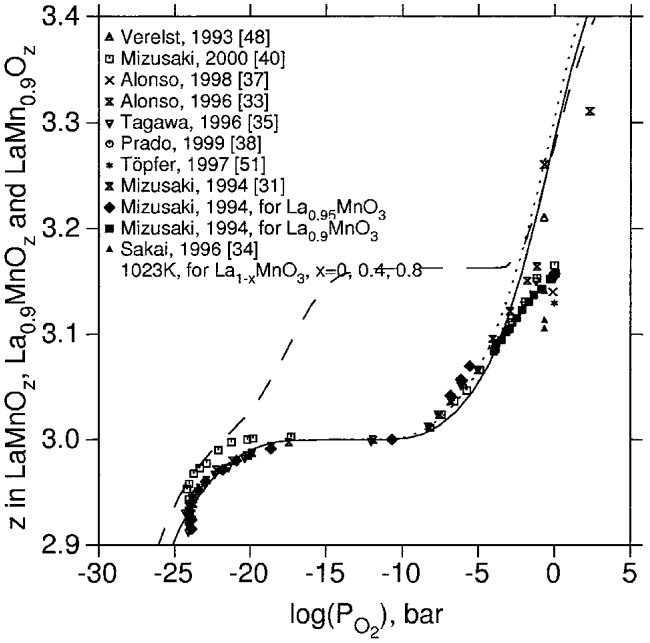

Fig. 12 The O content of $LaMnO_{3\pm\delta}$ (solid line), $LaMn_{0.9}O_{3\pm\delta}$ (dashed line), and $La_{0.9}MnO_{3\pm\delta}$ (dotted line) calculated as a function of $\log(P_{O2})$ at 973 K compared with data from the literature

number of measurements, and it can be seen that there are quite significant differences among the results from different groups. As discussed in detail elsewhere,[114] the experimental data on O nonstoichiometry for the perovskites with La deficiency can only be reproduced when Mn^{3+} is allowed to from antisite defects on the La sublattice.

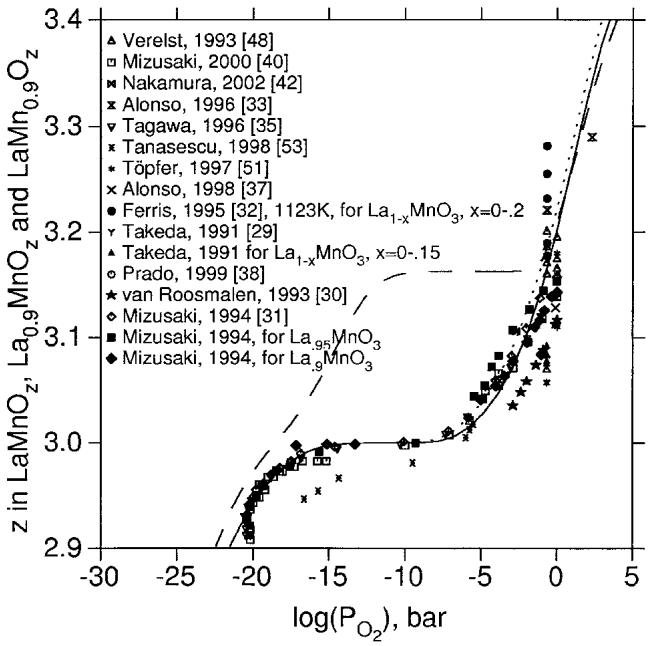

Fig. 13 The O content of $LaMnO_{3\pm\delta}$ (solid line), $LaMn_{0.9}O_{3\pm\delta}$ (dashed line), and $La_{0.9}MnO_{3\pm\delta}$ (dotted line) calculated as a function of $\log(P_{O2})$ at 1073 K compared with data from the literature

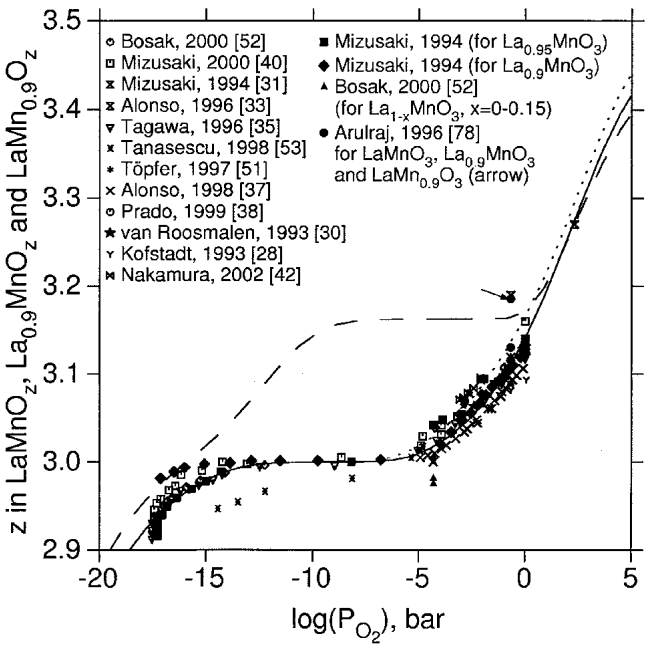

Fig. 14 The O content of $LaMnO_{3\pm\delta}$ (solid line), $LaMn_{0.9}O_{3\pm\delta}$ (dashed line), and $La_{0.9}MnO_{3\pm\delta}$ (dotted line) calculated as a function of $\log(P_{O2})$ at 1173 K compared with data from the literature

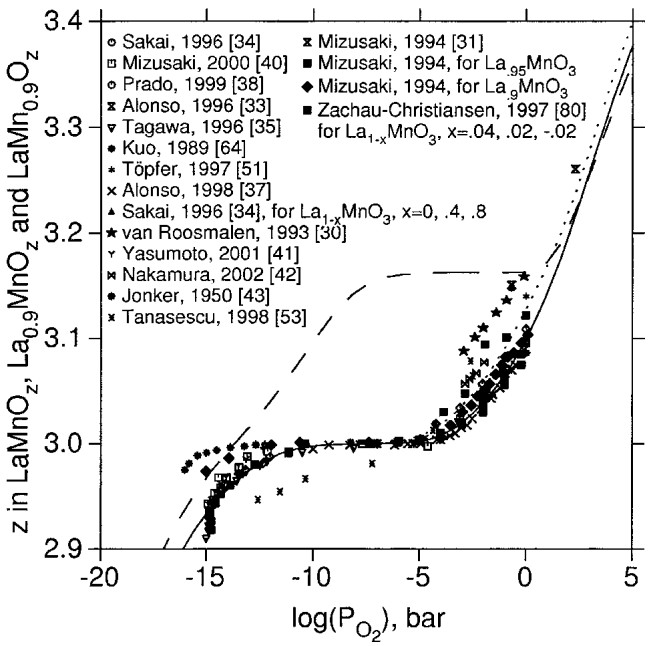

Fig. 15 The O content of $LaMnO_{3\pm\delta}$ (solid line), $LaMn_{0.9}O_{3\pm\delta}$ (dashed line), and $La_{0.9}MnO_{3\pm\delta}$ (dotted line) calculated as a function of $\log(P_{O2})$ at 1273 K compared with data from the literature

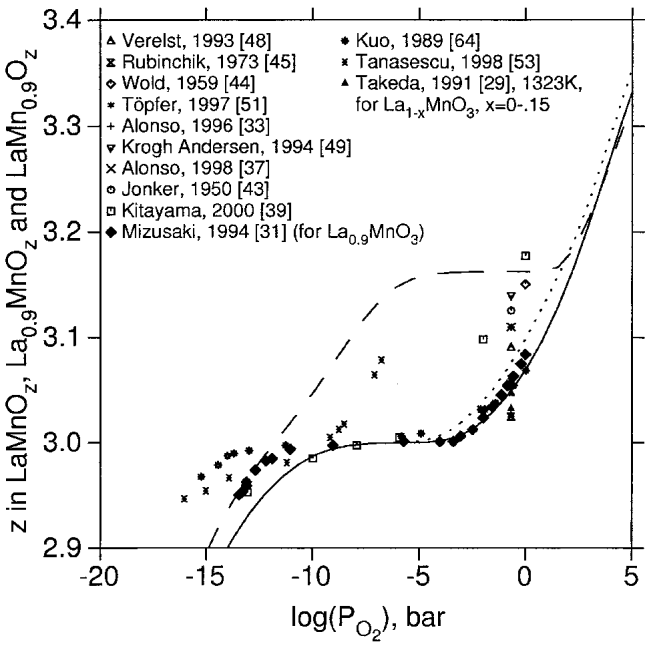

Fig. 16 The O content of $LaMnO_{3\pm\delta}$ (solid line), $LaMn_{0.9}O_{3\pm\delta}$ (dashed line), and $La_{0.9}MnO_{3\pm\delta}$ (dotted line) calculated as a function of $\log(P_{O2})$ at 1373 K compared with data from the literature

9.3 Calculated Site Fractions in the Perovskite $La_{1-x}Mn_{1-y}O_{3-z}$

The site fractions for the various ions in stoichiometric and La-deficient perovskite as a function of $\log(P_{O2})$ at 1273 K are shown in Fig. 19. In the stoichiometric perovskite (solid lines) between $\log(P_{O2})$ at approximately −12 and −1, it can be seen that there is a significant degree of charge disproportionation ($Mn^{3+} \rightarrow Mn^{2+} + Mn^{4+}$). This disproportionation is probably adequate to account for the good electrical conductivity of stoichiometric perovskites measured by van Roosmalen et al.[66] and Stevenson et

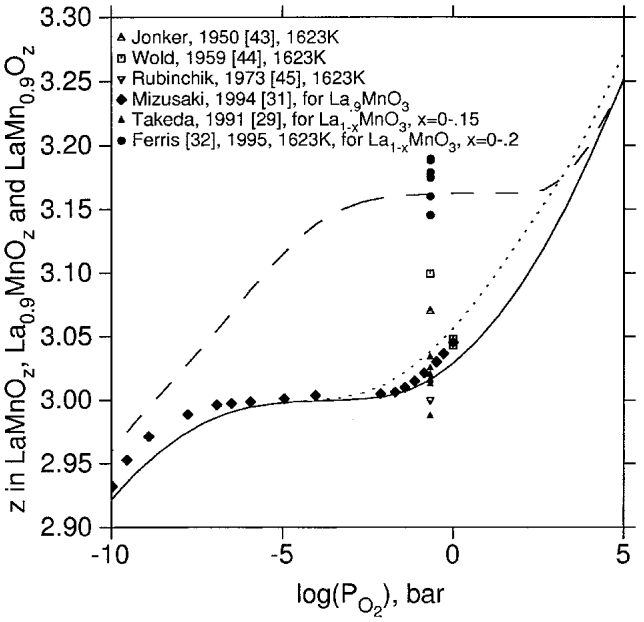

Fig. 17 The O content of $LaMnO_{3\pm\delta}$ (solid line), $LaMn_{0.9}O_{3\pm\delta}$ (dashed line), and $La_{0.9}MnO_{3\pm\delta}$ (dotted line) calculated as a function of $\log(P_{O2})$ at 1623 K compared with data from the literature

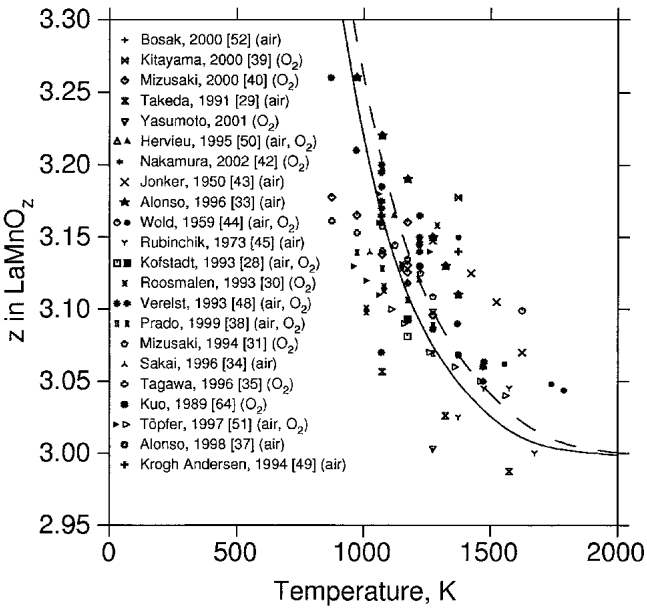

Fig. 18 Site fractions calculated for $La_{1-x}Mn_{1-y}O_{3-z}$ in air as a function of Mn content at 1273 K

al.[67,68] It can also be seen how the defect mechanism for La-deficient perovskites changes as a function of O partial pressure. At high O partial pressure, La deficiency is caused by excess La vacancies at low O partial pressures by Mn^{3+} sitting on La sites. A further point is that La deficiency does not lead to a large increase in Mn valency; Mn deficiency, on the other hand, does. This is in agreement with a large amount of qualitative data stating that La deficiency does not change the mean Mn valency, and also is in agreement

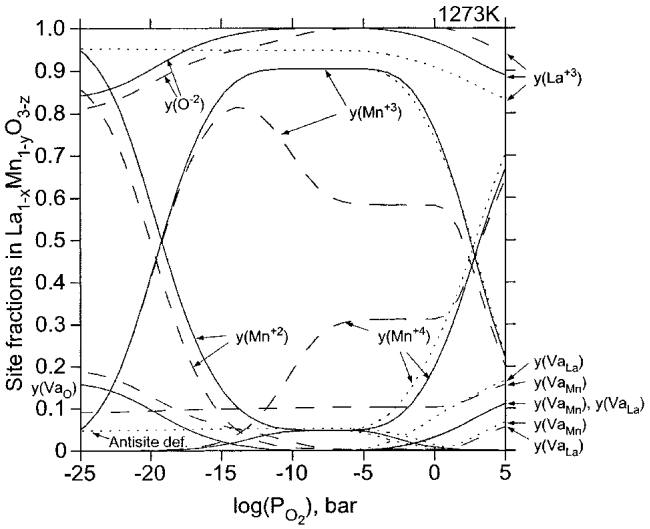

Fig. 19 Site fractions calculated for $LaMnO_{3\pm\delta}$ (solid line), $LaMn_{0.9}O_{3\pm\delta}$ (dashed line), and $La_{0.9}MnO_{3\pm\delta}$ (dotted line) at 1273 K as a function of $\log(P_{O2})$

with data from the study by Arulraj et al.,[78] who stated that Mn deficiency leads to a sharp increase in Mn valency.

Figure 20 shows the site fractions as a function of temperature for $LaMnO_{3\pm\delta}$, $La_{0.9}MnO_{3\pm\delta}$, and $LaMn_{0.9}O_{3\pm\delta}$ calculated in air. The trends are identical to the ones described in Fig. 19. Increasing the temperature at a constant O partial pressure corresponds to a lowering of the O partial pressure at a constant temperature. The equilibrium Mn valency in air below 600 K is 4+. In experiments, this value is, however, never reached due to kinetic reasons.

In the plot of site fractions as a function of cation fraction:

$$\frac{x(\mathrm{Mn})}{x(\mathrm{Mn}) + x(\mathrm{La})}$$

calculated at 1273 K in air (Fig. 21), it can be seen how La deficiency is first accomplished by the formation of La vacancies, and how later, for greater La deficiencies, Mn^{3+} antisite defects are formed and the Mn^{4+} content no longer increases.

From these calculations of site fractions as a function of O partial pressure, temperature, and cation composition, it can easily be seen that various defects are always at play simultaneously and that the relative importance of the defects change depending on the conditions. This complex defect behavior might offer an explanation for the ambiguous results found in literature.

10. Summary

Despite its relatively simple structure, the perovskite $La_{1-x}Mn_{1-y}O_{3-z}$ shows complicated defect chemistry, and quite a number of misconceptions and ambiguities can be found in literature. In this work, we have carefully reviewed

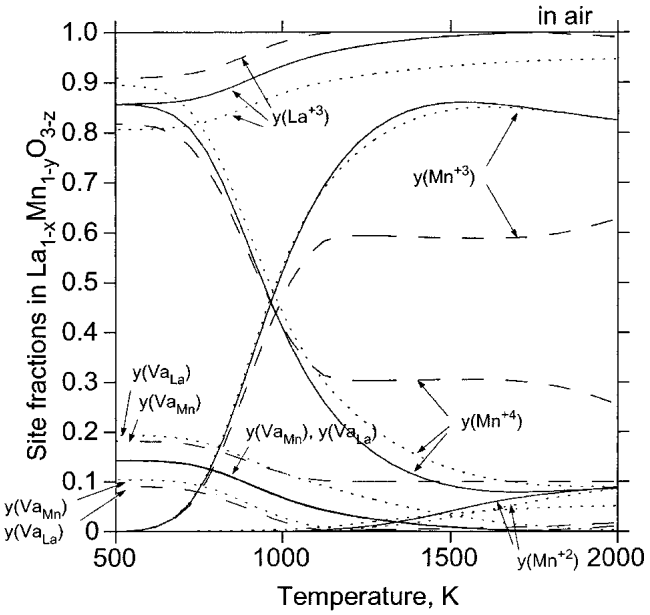

Fig. 20 Site fractions calculated for $LaMnO_{3\pm\delta}$ (solid line), $LaMn_{0.9}O_{3\pm\delta}$ (dashed line), and $La_{0.9}MnO_{3\pm\delta}$ (dotted line) in air as a function of temperature

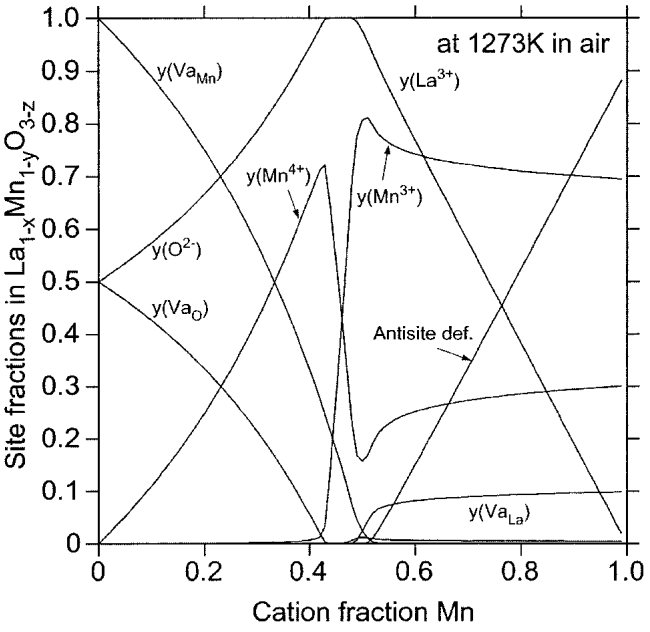

Fig. 21 Site fractions calculated for $La_{1-x}Mn_{1-y}O_{3-z}$ in air as a function of Mn content at 1273 K

the experimental data on the La-Mn-O system, in particular on the $La_{1-x}Mn_{1-y}O_{3-z}$ perovskite phase, and have chosen an appropriate model to describe the nonstoichiometry. This model includes Mn^{3+} antisite defects on the La sublattice. Consequently, using the compound energy formalism, the following sublattice occupation needs to be used: (La^{3+}, Mn^{3+}, Va)$_1$(Mn^{2+}, Mn^{3+}, Mn^{4+}, Va)$_1$(O^{2-}, Va)$_3$. As reported elsewhere,[114] only by choosing this sublattice model with Mn forming antisite defects on A-sites can the most reliable experimental data from the literature be reproduced. All other defect models inevitably lead to inconsistencies with some data from the literature. The ionic liquid is described using the two-sublattice model for ionic liquids with the sublattice occupation (La^{3+}, Mn^{2+}, Mn^{3+})$_p$(O^2, Va-^{q})$_q$. The model parameters were optimized using the CALPHAD approach.

References

1. C. Zener, Interaction between the d-Shells in the Transition Metals: II. Ferromagnetic Compounds of Manganese with Perovskite Structure, *Phys. Rev.,* Vol 82 (No. 3), 1951, p 403-405
2. J.B. Goodenough, Theory of the Role of Covalence in the Perovskite-Type Manganite [La, M(II)]MnO_3, *Phys. Rev.,* Vol 100 (No. 2), 1955, p 564–573
3. J.B. Goodenough, A. Wold, R.J. Arnott, and N. Menyuk, Relationship Between Crystal Symmetry and Magnetic Properties of Ionic Compounds Containing Mn^{3+}, *Phys. Rev.,* Vol 124 (No. 2), 1961, p 373-384
4. R.J.H. Voorhoeve, D.W. Johnson, J.P. Remeika, and P.K. Gallagher, Perovskite Oxides: Materials Science in Catalysis, *Science,* Vol 195 (No. 4281), 1977, p 827-833
5. N.Q. Minh, Ceramic Fuel Cells, *J. Am. Ceram. Soc.,* Vol 76 (No. 3), 1993, p 563-588
6. N.Q. Minh and T. Takahashi, *Science and Technology of Ceramic Fuel Cells*. Elsevier Science B.V., Amsterdam, The Netherlands, 1995
7. K. Chahara, T. Ohno, M. Kasai, and Y. Kozono, Magnetoresistance in Magnetic Manganese Oxide with Intrinsic Antiferromagnetic Spin Structure, *Appl. Phys. Lett.,* Vol 63 (No. 14), 1993, p 1990-1992
8. R. von Helmolt, J. Wecker, B. Holzapfel, L. Schulz, and K. Samwer, Giant Magnetoresistance in Perovskitelike $La_{2/3}Ba_{1/3}MnO_x$ Ferromagnetic Films, *Phys. Rev. Lett.,* Vol 17 (No. 14), 1993, p 2331-2333
9. R. Suryanarayanan, J. Berthon, I. Zelenay, B. Martinez, X. Obradors, S. Uma, and E. Gmelin, Giant Magnetoresistance, Thermoelectric Power and Specific Heat of $La_{1-y}MnO_3$, *Ceramics: Getting into the 2000's: Part A, Proceedings of the World Ceramics Congress, part of the 9th CIMTEC; World Ceramics Congress and Forum on New Materials*, *Advances in Science and Technology,* Vol 17. P. Vincenzini, Ed., Techna Srl., 1999, p 321-328
10. S. Jin, T.H. Tiefel, M. McCormack, R.A. Fasnacht, R. Ramesh, and L.H. Chen, Thousandfold Change in Resistivity in Magnetoresistive La-Ca-Mn-O Films, *Science,* Vol 264, 1994, p 413-415
11. E. Dagotta, T. Hotta, and A. Moreo, Colossal Magnetoresistant Materials: The Key Role of Phase Separation, *Phys. Rep.,* Vol 344, 2001, p 1-153
12. R. Mahendiran, S.K. Tiwary, A.K. Raychaudhuri, T.V. Ramakrishnan, R. Mahesh, N. Rangavittal, and C.N.R. Rao, Structure, Electron-Transport Properties, and Giant Magnetoresistance of Hole-Doped $LaMnO_3$ Systems, *Phys. Rev. B: Condens. Mater,* Vol 53 (No. 6), 1996, p 3348-3358
13. H.G. Jonker, Magnetic Compounds with Perovskite Structure IV, *Physica,* Vol 22, 1956, p 707-722
14. A.K. Bogush, V.I. Pavlov, and L.V. Balyko, Structural Phase Transitions in the $LaMnO_{3+\lambda}$ System, *Cryst. Res. Technol.,* Vol 18 (No. 5), 1983, p 589-598
15. D. Balz and K. Plieth, The Structure of Potassium Nickel

Fluoride, K_2NiF_4, *Z. Elektrochem.,* Vol 59 (No. 6), 1955, p 545-551
16. E.M. Vogel and D.W. Johnson, The Reduction of Alkali Substituted $LaMnO_3$, *Thermochim. Acta,* Vol 12, 1974, p 49-55
17. J. Sieler and J. Kaiser, Structure and Properties of Ternary and Quaternary Rare Earth-Transition Metal-Oxide Systems of the Type K_2NiF_4 and $CaFe_2O_4$, *Z. Anorg. Allg. Chem.,* 1970, Vol 377, p 316-320 (in German)
18. S.A. Nedilko, V.V. Pavlishchuk, and N.P. Zyryanova, Rare-Earth Element Manganates of Composition $LnMn_2O_5$, *Ukr. Khim. Zh. (Russ. Ed.),* Vol 46 (No. 11), 1980, p 1137-1140
19. B. Bochu, J. Chenavas, J.C. Joubert, and M. Marezio, High Pressure Synthesis and Crystal Structure of a New Series of Perovskiste-Like Compounds CMn_7O_{12} (C = Na, Ca, Cd, Sr, La, Nd), *J. Solid State Chem.,* Vol 11, 1974, p 88-93
20. J.B.A.A. Elemans, B. Van Laar, K.R. Van der Veen, and B.O. Loopstra, The Crystallographic and Magnetic Structures of $La_{1-x}BaxMn_{1-x}Me_xO_3$ (Me = Mn or Ti), *J. Solid State Chem.,* Vol 3, 1971, p 238-242
21. P. Norby, I.G. Krogh Andersen, E. Krogh Andersen, and N.H. Andersen, The Crystal Structure of Lanthanum Manganate(III), $LaMnO_3$, at Room Temperature and at 1273 K under N_2, *J. Solid State Chem.,* Vol 119, 1995, p 191-196
22. A.N. Grundy, B. Hallstedt, and L.J. Gauckler, Thermodynamic Assessment of the Lanthanum–Oxygen System, *J. Phase Equilib.,* Vol 22 (No. 2), 2001, p 105-113
23. A.N. Grundy, B. Hallstedt, and L. J.Gauckler, Assessment of the Mn–O System, *J. Phase Equilib.,* Vol 24 (No. 1), 2003, p 21-39
24. M. Hillert, The Compound Energy Formalism, *J. Alloys Compd.,* Vol 320, 2001, p 161-176
25. K. Frisk and M. Selleby, The Compound Energy Formalism: Applications, *J. Alloys Compd.,* Vol 320, 2001, p 177-188
26. M. Hillert, B. Jansson, B. Sundman, and J. Ågren, A Two-Sublattice Model for Molten Solutions with Different Tendency for Ionization, *Metall. Trans. A,* Vol 16A (No. 2), 1985, p 261-266
27. B. Sundman, Modification of the Two-Sublattice Model for Liquids, *CALPHAD,* Vol 15 (No. 2), 1991, p 109-119
28. P. Kofstad and A. Petrov, On the Defect Structure and Nonstoichiometry in Doped Perovskites: $La_{1-x}Sr_xMnO_{3\pm\delta}$, *High Temperature Electrochemical Behaviour of Fast Ion and Mixed Conductors*, *Proceedings of the 14th International Symposium on Materials Science,* F.W. Poulsen, Ed., 1993, p 287-296
29. Y. Takeda, S. Nakai, T. Kojima, N. Imanishi, G.Q. Shen, O. Yamamoto, M. Mori, C. Asakawa, and T. Abe, Phase Relation in the System $(La_{1-x}A_x)_{1-y}MnO_{3+z}$ (A = Sr and Ca), *Mater. Res. Bull.,* Vol 26, 1991, p 153-162
30. J.A.M. van Roosmalen and E.H.P. Cordfunke, Defect Chemical Properties of $(La,Sr)MnO_{3-\delta}$, *High Temperature Electrochemical Behaviour of Fast Ion and Mixed Conductors*, *Proceedings of the 14th International Symposium on Materials Science,* F.W. Poulsen, Ed., 1993, p 397-402
31. J. Mizusaki, H. Tagawa, Y. Yonemura, H. Minamiue, and H. Nambu, Effect of Lanthanum Deficiency on the Nonstoichiometry, Electronic Properties and Structure of $La_{1-x}MnO_{3+d}$, *Ionic and Mixed Conducting Ceramics*, *The Electrochem. Soc. Proc.,* Vol 94-12, T.A. Ramanarayanan, W.L. Worrell and H.L. Tuller, Ed., The Electrochemical Society, 1994, p 402-411
32. V. Ferris, L. Brohan, M. Ganne, and M. Tournoux, Structural Aspects, Density Measurements and Susceptibility Behavior of the Defect Perovskite $LaMnO_3$ with $0.8 \leq La/Mn \leq 1$ and $2.8 \leq O/Mn \leq 3.58$, *Eur. J. Solid State Inorg. Chem.,* Vol 32, 1995, p 131-144
33. J.A. Alonso, M.J. Martìnez-Lope, and M.T. Casais, High Oxygen Pressure Synthesis of $LaMnO_{3+\delta}$ with high δ Values ($\delta \leq 0.31$), *Eur. J. Solid State Inorg. Chem.,* Vol 33, 1996, p 331-341
34. N. Sakai and H. Fjellvåg, Effect of Non–Stoichiometry on Properties of $La_{1-t}MnO_{3-\delta}$: I. Phase Relations, *Acta Chem. Scand.,* Vol 50, 1996, p 580-586
35. H. Tagawa, J. Mizusaki, H. Takai, Y. Yonemura, H. Minamiue, and T. Hashimoto, Oxygen Hyperstoichiometry in Perovskite-Type Oxide, Undoped and Sr-Doped $LaMnO_3$, *High Temperature Electrochemistry: Ceramics and Metals*, *Proceedings of the 17th International Symposium on Materials Science,* F.W. Poulsen, N. Bonanos, S. Linderoth, M. Morgensen, and B. Zachau-Christiansen, Ed., 1996, p 437-442
36. H. Taguchi, S. Matsuura, M. Nagao, T. Choso, and K. Tabata, Synthesis of $LaMnO_{3+\delta}$ by Firing Gels Using Citric Acid, *J. Solid State Chem.,* Vol 129, 1997, p 60-65
37. J.A. Alonso, Non-Stoichiometry and Properties of Mixed Valence Manganites, *Philos. Trans. R. Soc. London*, *Ser. A,* Vol A356, 1998, p 1617-1634
38. F. Prado, R.D. Sánchez, A. Caneiro, M.T. Causa, and M. Tovar, Discontinuous Evolution of the Highly Distorted Orthorhombic Structure and the Magnetic Order in $LaMnO_{3\pm\delta}$ Perovskite, *J. Solid State Chem.,* Vol 146, 1999, p 418-427
39. K. Kitayama, Phase Equilibria in the System Ln-Mn-O, *J. Solid State Chem.,* Vol 153, 2000, p 336-341
40. J. Mizusaki, N. Mori, H. Takai, Y. Yonemura, H. Minamiue, H. Tagawa, M. Dokiya, H. Inaba, K. Naraya, T. Sasamoto, and T. Hashimoto, Oxygen Nonstoichiometry and Defect Equilibrium in the Perovskite-Type Oxides $La_{1-x}Sr_xMnO_{3+d}$, *Solid State Ionics,* Vol 129, 2000, p 163-177
41. K. Yasumoto, N. Mori, J. Mizusaki, H. Tagawa, and M. Dokiya, Effects of Oxygen Nonstoichiometry of Electrode Activity of $La_{1-x}A_xMnO_{3\pm\delta}$, *J. Electrochem. Soc.,* Vol 148 (No. 1), 2001, p A101-A111
42. K. Nakamura and K. Ogawa, Excess Oxygen in $LaMnO_{3-\delta}$, *J. Solid State Chem.,* Vol 163, 2002, p 65-76
43. G.H. Jonker and J.H. van Santen, Ferromagnetic Compounds of Manganese with Perovskite Structure, *Physica,* Vol 16 (No. 3), 1950, p 337-349
44. A. Wold and R.J. Arnott, Preparation and Crystallographic Properties of the Systems $LaMn_{1-x}Mn_xO_{3+\lambda}$ and $LaMn_{1-x}Ni_xO_{3+\lambda}$, *J. Phys. Chem. Solids,* Vol 9, 1959, p 176-180
45. Y.S. Rubinchik, S.A. Prokudina, and M.M. Pavlyuchenko, Synthesis and Formation Kinetics of $LaMnO_3$ in the Solid Phase, *Neorg. Mater.,* Vol 9 (No. 11), 1973, p 1732-1736
46. R.J.H. Voorhoeve, J.P. Remeika, L.E. Trimble, A.S. Cooper, F.J. Disalvo, and P.K. Gallagher, Perovskite-Like $La_{1-x}K_xMnO_3$ and Related Compounds: Solid State Chemistry and the Catalysis of the Reduction of NO by CO and H_2, *J. Solid State Chem.,* Vol 14, 1975, p 395-406
47. M. Ippommatsu, S. Otoshi, H. Sasaki, H. Ohnishi, T. Higuchi, M. Miyayama, and H. Yanagida, Study of $La_{1-x}MnO_{3\pm\delta}$ Non-Stoichiometry and Defect Structure using ESR and Iodometry, *J. Mater. Sci.,* Vol 28, 1993, p 4689-4692
48. M. Verelst, N. Rangavittal, C.N.R. Rao, and A. Rousset, Metal–Insulator Transition in Anion–Excess $LaMnO_{3-\delta}$ Controlled by the Mn^{4+} Content, *J. Solid State Chem.,* Vol 104, 1993, p 74-80
49. G. Krogh Andersen, I.E. Krogh Andersen, P. Norby, and E. Skou, Determination of Stoichiometry in Lanthanum Strontium Manganites(III)(IV) by Wet Chemical Methods, *J. Solid State Chem.,* Vol 113, 1994, p 320-326

50. M. Hervieu, R. Mahesh, N. Rangavittal, and C.N.R. Rao, Defect Structure of $LaMnO_3$, *Eur. J. Solid State Inorg. Chem.,* Vol 32 (No. 2), 1995, p 79-94
51. J. Töpfer and J.B. Goodenough, $LaMnO_{3+\delta}$ Revisited, *J. Solid State Chem.,* Vol 130, 1997, p 117-128
52. A.A. Bosak, O.Y. Gorbenko, A.R. Kaul, I.E. Graboy, C. Dubourdieu, J.P. Senateur, and H.W. Zandbergen, Cation and Oxygen Nonstoichiometry in R-Mn-O (R = La, Nd) Bulk Samples and Thin Films, *J. Magn. Magn. Mater.,* Vol 211, 2000, p 61-66
53. S. Tanasescu, N. Totir, and D.I. Marchidan, Thermodynamic Data of Perovskite-Type $LaMnO_{3\pm x}$ and $La_{0.7}Sr_{0.3}MnO_{3\pm x}$ by a Solid-State Electrochemical Technique, *Electrochim. Acta,* Vol 43 (No. 12–13), 1998, p 1675-1681
54. K. Kamata, T. Nakajima, T. Hayashi, and T. Nakamura, Nonstoichiometric Behavior and Phase Stability of Rare-Earth Manganites at 1200 °C, *Mater. Res. Bull.,* Vol 12, 1978, p 49-54
55. M.L. Borlera and F. Abbattista, Investigations of the La-Mn-O System, *J. Less-Common Met.,* Vol 92, 1983, p 55-65
56. T. Atsumi, T. Ohgushi, H. Namikata, and N. Kamegashira, Oxygen Nonstoichiometry of $LnMnO_{3-\delta}$ (Ln = La, Pr, Nd, Sm, and Y), *J. Alloys Compd.,* Vol 252, 1997, p 67-70
57. J.A.M. van Roosmalen and E.H.P. Cordfunke, The Defect Chemistry of $LaMnO_{3\pm\delta}$, 3. The Density of (La, *A*)$MnO_{3+\delta}$ (*A* = Ca, Sr, Ba), *J. Solid State Chem.,* Vol 110, 1994, p 106-108
58. B.C. Tofield and W.R. Scott, Oxidative Nonstoichiometry in Perovskites, an Experimental Survey; the Defect Structure of an Oxidized Lanthanum Manganite by Powder Neutron Diffraction, *J. Solid State Chem.,* Vol 10, 1974, p 183-194
59. J.A.M. van Roosmalen, E.H.P. Cordfunke, R.B. Helmholdt, and H.W. Zandbergen, The Defect Chemistry of $LaMnO_{3\pm\delta}$, 2. Structural Aspects of $LaMnO_{3\pm\delta}$, *J. Solid State Chem.,* Vol 110, 1994, p 100-105
60. J.F. Mitchell, D.N. Argyriou, C.D. Potter, D.G. Hinks, J.D. Jorgensen, and S.D. Bader, Structural Phase Diagram of $La_{1-x}Sr_xMnO_{3+\delta}$: Relationship to Magnetic and Transport Properties, *Phys. Rev. B,* Vol 54 (No. 9), 1996, p 6172-6183
61. J.A. Alonso, M.J. Martínez, M.T. Casais, J.L. MacManus-Driscoll, P.S.I.P.N. de Silva, L.F. Cohen, and M.T. Fernández-Díaz, Non–Stoichiometry, Structural Defects and Properties of $LaMnO_{3+\delta}$ with High δ Values ($0.11 \leq \delta \leq 0.29$), *J. Mater. Chem.,* Vol 7 (No. 10), 1997, p 2139-2144
62. Q. Huang, A. Santoro, J.W. Lynn, R.W. Erwin, J.A. Borchers, J.L. Peng, and R.L. Greene, Structure and Magnetic Order in Undoped Lanthanum Manganite, *Phys. Rev. B: Condens. Matter,* Vol 55 (No. 22), 1997, p 14987-14999
63. R.A. De Souza, M.S. Islam, and E. Ivers-Tiffée, Formation and Migration of Cation Defects in the Perovskite Oxide $LaMnO_3$, *J. Mater. Chem.,* Vol 9 (No. 7), 1999, p 1621-1627
64. J.H. Kuo, H.U. Anderson, and D.M. Sparlin, Oxidation–Reduction Behavior of Undoped and Sr-Doped $LaMnO_3$ Nonstoichiometry and Defect Structure, *J. Solid State Chem.,* Vol 83, 1989, p 52-60
65. J.A.M. van Roosmalen and E.H.P. Cordfunke, The Defect Chemistry of $LaMnO_{3\pm\delta}$, 4. Defect Model for $LaMnO_{3\pm\delta}$, *J. Solid State Chem.,* Vol 110, 1994, p 109-112
66. J.A.M. van Roosmalen, J.P.P. Huijsmans, and L. Plomp, Electrical Conductivity in $La_{1-x}Sr_xMnO_{3+\delta}$, *Solid State Ionics,* Vol 66, 1993, p 279-284
67. J.W. Stevenson, M.M. Nasrallah, H.U. Anderson, and D.M. Sparlin, Defect Structure of $Y_{1-y}Ca_yMnO_3$ and $La_{1-y}Ca_yMnO_3$: I. Electrical Properties, *J. Solid State Chem.,* Vol 102, 1993, p 175-184
68. J.W. Stevenson, M.M. Nasrallah, H.U. Anderson, and D.M. Sparlin, Defect Structure of $Y_{1-y}Ca_yMnO_3$ and $La_{1-y}Ca_yMnO_3$: II. Oxidation: Reduction Behavior, *J. Solid State Chem.,* Vol 102, 1993, p 185-197
69. J. Mizusaki, Y. Yonemura, H. Kamata, K. Ohyama, N. Mori, H. Takai, H. Tagawa, M. Dokiya, K. Naraya, T. Sasamoto, H. Inaba, and T. Hashimoto, Electronic Conductivity, Seebeck Coefficient, Defect and Electronic Structure of Nonstoichiometric $La_{1-x}Sr_xMnO_3$, *Solid State Ionics,* Vol 132, 2000, p 167-180
70. R.E. Cook, K.C. Goretta, J. Wolfenstine, P. Nash, and J.L. Routbort, High-Temperature Deformation and Defect Chemistry of $La_{1-x}Sr_xMnO_{3+\delta}$, *Acta Mater.,* Vol 47 (No. 10), 1999, p 2969-2980
71. I. Maurin, P. Barboux, Y. Lassailly, J.-P. Boilot, and F. Villain, Charge–Carrier Localization in the Self-Doped $La_{1-y}Mn_{1-y}O_3$ System, *J. Magn. Magn. Mater.,* Vol 211, 2000, p 139-144
72. J.A.M. van Roosmalen and E.H.P. Cordfunke, Chemical Reactivity and Interdiffusion of (La, Sr)MnO_3 and (Zr, Y)O_2, Solid Oxide Fuel Cell Cathode and Electrolyte Materials, *Solid State Ionics,* Vol 52, 1992, p 303-312
73. A. Mitterdorfer and L.J. Gauckler, $La_2Zr_2O_7$ formation and oxygen reduction kinetics of the $La_{0.85}Sr_{0.15}Mn_yO_3$, $O_2(g)$ | YSZ system, *Solid State Ionics,* Vol 111, 1998, p 185-218
74. S.P. Jiang, J.G. Love, J.P. Zhang, M. Hoang, Y. Ramprakash, A.E. Hughes, and S.P.S. Badwal, The Electrochemical Performance of LSM/Zirconia–Yttria Interface as a Function of A-Site Non-Stoichiometry and Cathodic Current Treatment, *Solid State Ionics,* Vol 121, 1999, p 1-10
75. M. Mori, T. Abe, H. Itoh, O. Yamamoto, G.Q. Shen, Y. Takeda, and N. Imanishi, Reaction Mechanism Between Lanthanum Manganite and Yttria Doped Cubic Zirconia, *Solid State Ionics,* Vol 123, p 113-119
76. S. Habekost, P. Norby, J.E. Jorgensen, and B. Lebech, Neutron and X-ray Powder Diffraction Studies of Lanthanum Manganite Perovskite, *Acta Chem. Scand.,* Vol 48 (No. 5), 1994, p 377-381
77. S. Hébert, B. Wang, A. Maignan, C. Martin, R. Retoux, and B. Raveau, Vacancies at Mn-Site in Mn^{3+} Rich Manganites: A Route to Ferromagnetism but Not to Metallicity, *Solid State Commun.,* Vol 123 (No. 6-7), 2002, p 311-315
78. A. Arulraj, R. Mahesh, G.N. Subbanna, R. Mahendiran, A.K. Raychaudhuri, and C.N.R. Rao, Insulator–Metal Transitions, Giant Magnetoresistance, and Related Aspects of the Cation-Deficient $LaMnO_3$ Compositions $La_{1-\delta}MnO_3$ and $LaMn_{1-\delta}O_3$, *J. Solid State Chem.,* Vol 127, 1996, p 87-91
79. J.A.M. van Roosmalen, P. van Vlaanderen, E.H.P. Cordfunke, W.L. Ijdo, and D.J.W. Ijdo, Phases in the Perovskite-Type $LaMnO_{3+\delta}$ Solid Solution and the La_2O_3-Mn_2O_3 Phase Diagram, *J. Solid State Chem.,* Vol 114, 1995, p 516-523
80. B. Zachau-Christiansen, T. Jacobsen, and S. Skaarup, Oxygen Stoichiometry in Cation Deficient $(La,Sr)_{1-z}MnO_3$ SOFC Cathode Materials, *Solid Oxide Fuel Cells V (SOFC-V), The Electrochem. Soc. Proc.,* Vol 97-40 or 97-18, U. Stimming, S.C. Singhal, H. Tagawa, and W. Lehnert, The Electrochemical Society, 1997, p 795–804
81. R.D. Shannon, Revised Effective Ionic Radii and Systematic Atudies of Interatomic Distances in Halides and Chalcogenides, *Acta Crystallogr.,* Vol A32, 1976, p 751-767
82. N. Sakai, H. Fjellvåg, and B. Lebech, Effect of Non-Stoichiometry on Properties of $La_{1-t}MnO_{3+\delta}$: Part II. Crystal Structure, *Acta Chem. Scand.,* Vol 51 (No. 9), 1997, p 904-909
83. H. Cerva, Imaging of La/Sr Vacancy Defects in $La_{0.8}Sr_{0.2}MnO_3$ by High–Resolution Transmission Electron Microscopy, *J. Solid State Chem.,* Vol 114, 1995, p 211-218

84. M. Wolcyrz, R. Horyn, F. Bourée, and E. Bukowska, Structural Defects in $LaMnO_3$ Phase Studied by Neutron Diffraction, *J. Alloys Compd.,* Vol 353, 2003, p 170-174
85. R. Horyn, A. Sikora, and E. Bukowska, Polymorphic Forms and Defect Structure Formation within Homogeneity Domain of $LaMnO_3$ Phase, *J. Alloys Compd.,* Vol 353, 2003, p 153-169
86. J.A.M. van Roosmalen, E.H.P. Cordfunke, and J.P.P. Huijsmans, Sinter Behavior of (La, Sr)MnO_3, *Solid State Ionics,* Vol 66, 1993, p 285-293
87. J.W. Stevenson, P.F. Hallmann, T.R. Armstrong, and L.A. Chick, Sintering Behavior of Doped Lanthanum and Yttrium Manganite, *J. Am. Ceram. Soc.,* Vol 78 (No. 3), 1995, p 507-512
88. A.V. Berenov, J.L. MacManus-Driscoll, and J.A. Kilner, Oxygen Tracer Diffusion in Undoped Lanthanum Manganites, *Solid State Ionics,* Vol 122, 1999, p 41-49
89. H. Jena, K.V. Govindan Kutty, and T.R.N. Kutty, Studies on the Structural and Ionic Transport Properties at Elevated Temperatures of $La_{1-x}MnO_{3-\delta}$ Synthesized by a Wet Chemical Method, *J. Alloys Compd.,* Vol 350, 2003, p 102-112
90. J. Töpfer and J.B. Goodenough, Charge Transport and Magnetic Properties in Perovskites of the System La-Mn-O, *Solid State Ionics,* Vol 101-103, 1997, p 1215-1220
91. V.P. Pashchenko, S.I. Khartsev, O.P. Cherenkov, A.A. Shemyakov, A.D. Loiko, and V.I. Kamenev, Nonstoichiometry, Structural Perfection, and Properties of $La_{1-x}Mn_{1+x}O_{3\pm\delta}$ Magnetoresistive Materials, *Inorg. Mater.,* Vol 35 (No. 12), 1999, p 1294-1300
92. H.W. King, K.M. Castelliz, G.J. Murphy, and W. Manuel, The Effect of B-Metal Substitution on the Structure and Electrical Resistivity of $LaMnO_3$ and $SrMnO_3$, *J. Can. Ceram. Soc.,* Vol 51, 1982, p 1-5
93. J.A. Alonso, M.T. Casais, M.J. Martínez, and M.T. Fernández-Díaz, A Structural Study from Neutron Diffraction Data and Magnetic Properties of RMn_2O_5 (Re = La, Rare Earth), *J. Phys.: Condens. Mater,* Vol 9, 1997, p 8515-8526
94. J.A. Alonso, M.T. Casais, M.J. Martínez-Lope, and I. Rasines, High Oxygen Pressure Preparation, Structural Refinement, and Thermal Behavior of RMn_2O_5 (R = La, Pr, Nd, Sm, Eu), *J. Solid State Chem.,* Vol 129, 1997, p 105-112
95. F. Abbattista and M.L. Borlera, Reduction of $LaMnO_3$. Structural Features of Phases $La_8Mn_8O_{23}$ and $La_4Mn_4O_{11}$, *Ceram. Int.,* Vol 7 (No. 4), 1981, p 137-141
96. J.A.M. van Roosmalen and E.H.P. Cordfunke, A New Defect Model to Describe the Oxygen Deficiency in Perovskite-Type Oxides, *J. Solid State Chem.,* Vol 93, 1991, p 212-219
97. O.M. Sreedharan, R. Pankajavalli, and J.B. Gnanamoorthy, Standard Gibbs' Energy of Formation of $LaMnO_3$ from EMF Measurements, *High Temp. Sci.,* Vol 16, 1983, p 251-256
98. R. Hildrum, M. Brustad, and Ø. Johannesen, Thermodynamic Properties of Doped Lanthanum Manganites, *Mater. Res. Bull.,* Vol 29 (No. 8), 1994, p 851-860
99. T. Atsumi, T. Ohgushi, and N. Kamegashira, Studies on Oxygen Dissociation Pressure of $LnMnO_3$ (Ln = Rare Earth) with the e.m.f. Technique, *J. Alloys Compd.,* Vol 238, 1996, p 35-40
100. K.T. Jacob and M. Attaluri, Refinement of Thermodynamic Data for $LaMnO_3$, *J. Mater. Chem.*, Vol 13, 2003, p 934-942
101. Y.P. Vorob'ev, A.A. Novlev, S.A. Leont'ev, A.N. Men', S.A. Prokudina, and Y.S. Rubinchik, Thermodynamic Properties of $LaMnO_3$, *Neorg. Mater.,* Vol 15 (No. 8), 1979, p 1449-1453
102. T. Nakamura, G. Petzow, and L.J. Gauckler, Stability of the Perovskite Phase $LaBO_3$ (B = V, Cr, Mn, Fe, Co, Ni) in Reducing Atmospheres: I. Experimental Results, *Mater. Res. Bull.,* Vol 14, 1979, p 649-659
103. N. Kamegashira, Y. Miyazaki, and Y. Hiyoshi, Limiting Oxygen Partial Pressure of $LaMnO_3$ Phase, *Mater. Lett.,* Vol 2 (No. 3), 1984, p 194-195
104. C. Laberty, A. Navrotsky, C.N.R. Rao, and P. Alphonse, Energetics of Rare Earth Managanese Perovskites $A_{1-x}A'_xMnO_3$ (A = La, Nd, Y and A' = Sr, La) Systems, *J. Solid State Chem.,* Vol 145, 1999, p 77-87
105. L. Rørmark, S. Stølen, K. Wiik, and T. Grande, Enthalpies of Formation of $La_{1-x}A_xMnO_{3\pm\delta}$ (A = Ca and Sr) Measured by High–Temperature Solution Calorimetry, *J. Solid State Chem.,* Vol 163, 2002, p 186-193
106. H. Yokokawa, N. Sakai, T. Kawada, and M. Dokiya, Chemical Potential Diagram for Rare Earth-Transition Metal-Oxygen System: I, Ln-V-O and Ln-Mn-O Systems, *J. Am. Ceram. Soc.,* Vol 73 (No. 3), 1990, p 649-658
107. H. Satoh, M. Takagi, K. Kinukawa, and N. Kamegashira, Heat Capacity of $LaMnO_3$, *J. Therm. Anal.,* Vol 299, 1997, p 123-126
108. M. Temkin, Mixtures of Fused Salts as Ionic Solutions, *Acta Physicochim. URSS,* Vol 20 (No. 4), 1945, p 411-420
109. A.T. Dinsdale, SGTE Data for Pure Elements, *CALPHAD,* Vol 15 (No. 4), 1991, p 317-425
110. O. Redlich and A.T. Kister, Algebraic Representation of Thermodynamic Properties and the Classification of Solutions, *Ind. Eng. Chem.,* Vol 40 (No. 2), 1948, p 345-348
111. E.A. Guggenheim, The Theoretical Basis of Raoult's Law, *Trans. Faraday Soc.,* Vol 33, 1937, p 151-156
112. S. Tanasescu, Unpublished Measurements on La_2MnO_4, Institute of Physical Chemistry "I.G. Murgulesca" of the Romanian Academy, *personal communication,* 2002
113. B. Sundman, B. Jansson, and J.-O. Andersson, The Thermo-Calc Databank System, *CALPHAD,* Vol 9 (No. 2), 1985, p 153-190
114. A.N. Grundy, B. Hallstedt, and L.J. Gauckler, $La_{1-x}Mn_{1-y}O_{3-z}$ Perovskites Modelled with and without Antisite Defects Using the CALPHAD Approach, *Solid State Ionics,* Vol 173, 2004, p 17-21